

Air Force Institute of Technology

AFIT Scholar

Theses and Dissertations

Student Graduate Works

3-22-2012

Turbulence Measurement in the Atmospheric Boundary Layer Using Cellular Telephone Signals

Lee R. Burchett

Follow this and additional works at: <https://scholar.afit.edu/etd>



Part of the [Meteorology Commons](#)

Recommended Citation

Burchett, Lee R., "Turbulence Measurement in the Atmospheric Boundary Layer Using Cellular Telephone Signals" (2012). *Theses and Dissertations*. 1170.

<https://scholar.afit.edu/etd/1170>

This Thesis is brought to you for free and open access by the Student Graduate Works at AFIT Scholar. It has been accepted for inclusion in Theses and Dissertations by an authorized administrator of AFIT Scholar. For more information, please contact richard.mansfield@afit.edu.



**TURBULENCE MEASUREMENT IN THE ATMOSPHERIC
BOUNDARY LAYER USING CELLULAR TELEPHONE SIGNALS**

THESIS

Lee R. Burchett, Civilian
AFIT/APPLPHY/ENP/12 - M01

**DEPARTMENT OF THE AIR FORCE
AIR UNIVERSITY**

AIR FORCE INSTITUTE OF TECHNOLOGY

Wright-Patterson Air Force Base, Ohio

DISTRIBUTION STATEMENT A
APPROVED FOR PUBLIC RELEASE; DISTRIBUTION UNLIMITED

The views expressed in this document are those of the author and do not reflect the official policy or position of the United States Air Force, the United States Department of Defense or the United States Government. This material is declared a work of the U.S. Government and is not subject to copyright protection in the United States.

AFIT/APPLPHY/ENP/12 - M01

TURBULENCE MEASUREMENT IN THE ATMOSPHERIC BOUNDARY
LAYER USING CELLULAR TELEPHONE SIGNALS

THESIS

Presented to the Faculty
Department of Engineering Physics
Graduate School of Engineering and Management
Air Force Institute of Technology
Air University
Air Education and Training Command
in Partial Fulfillment of the Requirements for the
Degree of Masters of Science in Applied Physics

Lee R. Burchett, BS

Civilian

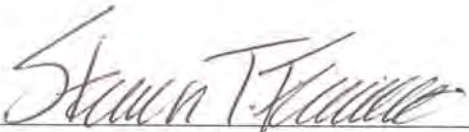
March 2012

DISTRIBUTION STATEMENT A
APPROVED FOR PUBLIC RELEASE; DISTRIBUTION UNLIMITED

TURBULENCE MEASUREMENT IN THE ATMOSPHERIC BOUNDARY
LAYER USING CELLULAR TELEPHONE SIGNALS

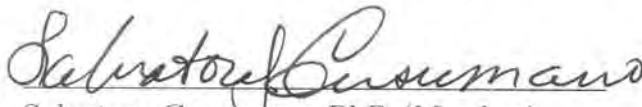
Lee R. Burchett, BS
Civilian

Approved:




Steven Fiorino, PhD (Chairman)

13 MAR 12
Date



Salvatore Cusumano, PhD (Member)

13 Mar 12
Date



Maj Mylo Hyde (Member)

13 Mar 12
Date

Abstract

A new method for measuring the intensity of turbulence in the planetary boundary layer was investigated, and showed high correlation with measurements from weather radar. This method takes measurements of cell phone signal strength and uses scintillation in the signal to estimate the strength of local turbulence. Using cell phone signals provides unique measurement advantages: it is a passive measurement method, it is not strongly affected by precipitation, and one device can potentially measure several paths at once. The measurements were taken using an Android[®] cell phone running a custom built application. Turbulence was quantified using the index of refraction structure constant, C_n^2 , which is related to the amount of energy in the turbulence. The goal of the investigation was to determine if C_n^2 values calculated from the cell phone signal power show a relationship to C_n^2 measurements taken over the communication path. Based on the strength of the agreement between measurements made by the new method and those done with an established method, it is concluded that turbulence changes can be measured using cell phone signals.

The correlation of C_n^2 values measured using the two methods was calculated for 42 periods of about 12 hours each. Correlation varied over the 42 periods, but was high and statistically significant in most measurements. The mean absolute value of peak Pearson correlation was 0.5865 with a mean p -value of 0.0251. Standard deviations of these values are 0.2311 and 0.0264, respectively. The standard deviations are relatively high due to two outliers where the correlation was particularly low. This thesis presents the experimental work that was done, the results of the work, the author's interpretation of the results, and suggestions for continued research.

Acknowledgements

I would like to thank God, who has given me everything I have, and allowed me to do this work; My parents for support and guidance that has brought me here today; My wife and family for their understanding, support, and inspiration throughout this research; All those who have come before me, and provided the innumerable tools and knowledge that I needed in order to do this work; My thesis committee for their indispensable guidance and support; The men and women of the United States armed forces for their sacrifices past and present; and The Air Force Institute of Technology and the Center for Directed Energy for supporting my work.

Lee R. Burchett

Table of Contents

	Page
Abstract	iv
Acknowledgements	v
List of Figures	viii
List of Tables	xii
List of Symbols	xiii
List of Abbreviations	xiv
I. Introduction	1
II. Theoretical Background	6
Turbulence and Structure Functions	6
Turbulence in the Planetary Boundary Layer	9
Refraction and Scintillation	14
Cell Phone Signal Characteristics	20
III. Experimental Design and Methods	24
Experiment Overview	24
Taking Measurements With The Phone	26
Taking Measurement With The Radar	31
Calculating and Comparing C_n^2 From Both Sources	33
File Selection	33
Calculating C_n^2 From Weather Radar	34
Calculating C_n^2 From Cell Phone Measurements	34
Automated Result Comparison	36
Manual Comparison	38
IV. Results	42
Correlation Results	42
Cross Correlation	42
Pearson, Spearman, and Kendall Correlations	54
Weather Effects	61
Weather During Good Correlation	61
Weather During Bad Correlation	63
Poor Correlation That May Not Be Directly Related to Weather	68

	Page
V. Conclusions and Suggestions for Further Work	71
Conclusions	71
Suggestions for Future Work	74
Verifying CDMA Hyper-Sensitivity	74
Appendix A. CDMA Encoding → Decoding	76
Appendix B. Phone Logging Application	82
Appendix C. Radar Data Extraction Library	85
Glossary	89
Bibliography	92

List of Figures

Figure		Page
1.	Four plots from the Wilmington Nexrad radar showing varied levels of clear air coverage. Clockwise from top left: Zoom of the Dayton area where measurements were taken with moderate coverage; Strong coverage with some range reduction due to the weather front; poor coverage that is possibly due to weather system to the south; Good coverage with long range.	4
2.	False color image of turbulence induced by a submerged jet made visible by laser induced fluorescence. The image is owned by C. Fukushima and J. Westerweel, Technical University of Delft, The Netherlands, and is used without permission or endorsement of this work under the Creative Commons license.	8
3.	Cartoon of index variance in plane transverse to the direction of propagation.	13
4.	Above: A receiver that is close enough to a transmitter so that the Fresnel zone, F , is less than the scale height. Below: Moving the same receiver away from the transmitter causes the Fresnel zone to grow larger than the turbulence scale height.	19
5.	Satellite image of Transmitter to Receiver path. The path length is 623 m. The distance from the KILN radar (not shown) is 42 km. Image copyright owned by ©Google 2011.	25
6.	Cartoon of a path passing through three bins.	32
7.	Three plots of C_n^2 Derived from cell phone signal power scintillation. The plots were each calculated from the same data set using different window sizes. From top to bottom, the window sizes are 300 s, 90 s, and 30 s. The data is from Monday, August 22, 8:37 pm EDT until August 23, 9:02 am.	35

Figure	Page	
8.	Top: Surface wind speed and solar elevation angle. Middle: Sun and wind data superimposed over normalized Voice and Data C_n^2 plots. Bottom: Sun and wind data superimposed over a normalized Radar C_n^2 plot. Time is local EDT, the plots begin August 17, 2011 at approximately 10:30 pm.....	37
9.	The top plot is an example cross-correlation. In the bottom plot, the absolute value of the correlation is taken, and the maximum value is picked out to be used as the cross-correlation for this data set.	43
10.	Four distributions of the measured correlation between 1200 sets of random data and C_n^2 measurements from Radar (Right Top and Right Bottom) and Voice (Left Top and Left Bottom). Normal distributions are superimposed in red.	45
11.	Left: Correlations of the various plots with any time lag. Right: The same correlations when with either 0 or -1 time lag.	46
12.	Lag at cross correlation peak. The lag values are normalized by dividing by the number of points.	47
13.	The peak correlation period in the CPSD of all 42 data sets.	49
14.	Top: The correlation coefficients for the three data sources are plotted. Bottom: The mean correlation coefficients of each data source and random data sets. All coefficients are normalized. Each of the three data sources was correlated with 112 random number sets. Values are taken from the zero-lag correlation, or the first set lags by 1 correlation: whichever is larger.	50
15.	Top: The maximum correlation coefficients for the three data sources are plotted. Bottom: The mean maximum correlation coefficients of each data source and random data sets. All coefficients are normalized. Each of the three data sources was correlated with 112 random number sets. The maximum is compared to correlations at all possible lag values.	51

Figure	Page
16. C_n^2 values from August 22 - 23. The second half of the plot shows many points where data was not available.	52
17. Pearson correlation of three C_n^2 data series to random data.	55
18. Correlation of Data and Voice measurements taken at zero lag.	55
19. Correlation of Data and Voice measurements taken at the lag where the cross-correlation peaks.	56
20. Correlation of Radar and Voice measurements taken at zero lag.	57
21. Correlation of Radar and Voice measurements taken at the lag where the cross-correlation peaks.	58
22. Correlation of Radar and Data measurements taken at zero lag.	58
23. Correlation of Radar and Data measurements taken at the lag where the cross-correlation peaks.	59
24. Cross correlation results with the 4 poor correlation plots circled in red, and the two high correlation plots circled in black. The data set numbers are in blue.	61
25. Normalized Radar and phone measurements of C_n^2 taken on August 7 th during a time of cloudy skies with light to moderate winds. These plots showed good overall correlation.	62
26. Normalized Radar and phone measurements of C_n^2 taken on August 27 th . The plots show good correlation.	63
27. Normalized Radar and phone measurements of C_n^2 . The shaded area indicates a period of reported thunderstorms.	64
28. Normalized Radar and phone measurements of C_n^2 . The shaded area indicates a period of reported mist.	65
29. Normalized Radar and phone measurements of C_n^2 . The shaded area indicates a period of strong winds.	66

Figure	Page
30. Normalized Radar and phone measurements of C_n^2 . The shaded area indicates a period of reported mist.....	67
31. Normalized Radar and phone measurements of C_n^2 . The plot characteristics change dramatically at approximately 7:00 am. This is approximately sunrise, and the wind speed dropped from a steady wind overnight to almost no winds during the day.	70
32. Cartoon of the process by which the Android phone updates the power level to the data logging software.	83
33. Wilmington NEXRAD Radar image showing clear air returns from the Miami Valley region. The red lines are major highways in the area.	86
34. Cartoon of a weather radar sweep. The azimuthal divisions of the sweeps are rays, and the radial divisions of the rays are bins. In each radar sweep it is possible for rays or bins to be missing. Also the spacing and number of bins varies from ray to ray, the spacing and number of rays varies from sweep to sweep.....	87

List of Tables

Table	Page
1. List of Correlation Comparisons	39
2. Some Basic Orthogonal Codes	78
3. The binary word 0110 0001 expanded out for encoding.	79
4. An example of encoding the binary word 0110 0001 with the user code 1001.	79
5. Combining several users' signals into one signal.	80
6. Decoding Data	80

List of Symbols

Symbol	Page
C_n^2	Index of Refraction Structure constant in $m^{-2/3}$ iv
V	Fluid Velocity 9
L	Characteristic Length for Fluid Flow 9
ν	Fluid Viscosity 9
L_0	Outer Scale of Turbulent Eddies 10
l_0	Inner scale of atmospheric turbulence 11
σ_n^2	Variance of the Index of Refraction 11
n	The index of refraction 11
Δx	Finite Difference 12
$\langle \rangle$	Mean, or Expected Value 12
F	Length of First Fresnel Zone 15
λ	Wavelength 15
k	Wavenumber $2\pi/\lambda$ 18
σ_1^2	Rytov Variance 18
σ_I^2	Scintillation Index 18
$R_{average}$	Reflectivity 31
K_w	Complex Index of Refraction of Water 34
dBz	Decibel Reflectivity 34

List of Abbreviations

Abbreviation	Page
DoD	United States Department of Defense 1
EM	Electromagnetic 2
RF	Radio Frequency 3
RHS	Right Hand Side 12
IR	Infra-Red 15
CDMA	Code Division Multiple Access 17
SDK	Software Development Kit 26
ERP	Effective Radiated Power 27
PCS	Personal Communication Service 27
GPS	Global Positioning System 30
AFIT	Air Force Institute of Technology 31
CDE	Center for Directed Energy 31
EDT	Eastern Daylight Time 36
Tx	Transmitter 76
Rx	Receiver 76
OS	Operating System 82
TRMM	Tropical Rainfall Measurement Mission 85
RSL	Radar Science Library 85

TURBULENCE MEASUREMENT IN THE ATMOSPHERIC BOUNDARY LAYER USING CELLULAR TELEPHONE SIGNALS

I. Introduction

What follows is an introduction to the motivation for this research; the concepts and terminology that will be used; and a brief survey of similar research. The next chapter will provide a more detailed background on turbulence in general, turbulence in the *boundary layer*, scintillation from turbulence, the C_n^2 parameter, and the relevant characteristics of the cell phone signals that will be used. Chapter III will discuss the measurement method. This will include a description of the equipment used, the sources of weather and radar data, software that was written, and the processes used in taking and comparing measurements. In Chapter IV the measurements will be presented, along with their interpretation and statistical analysis. Measurements will also be compared with local weather events, and the chapter will address plots with low correlation. The final chapter includes the conclusions drawn from this work, and suggestions for follow-on research. Because some terms used in this text have multiple meanings or interpretations and to help with technical terms that are not widely known, a glossary is provided with intended definitions of these terms. These terms will be written in italics when they first appear in a chapter. Several appendixes are provided as well for ancillary information about the experiment.

Understanding and measuring turbulence within the (planetary) boundary layer is important for improving the effectiveness of many DoD systems. The boundary layer is the lowest atmospheric layer, and is where almost all human activity occurs. In this layer, temperature, pressure, and humidity variations affect the index of re-

fraction of air leading to amplitude and phase scintillation in EM waves [2] [15] [6]. Understanding the effects and current state of turbulence in the boundary layer is important to the continued development and improvement of directed energy weapons, communications, navigation, and remote sensing systems.

Knowing the energy profile of turbulence allows for a more accurate estimation of how well many DoD systems will perform. This can provide more efficient use of these systems. For example, the effective range of a laser weapon is limited by the strength of turbulence on the path to the target. Knowing the intensity of turbulence allows a laser to be used at maximum range with less chance of wasting a pulse when the probability of a kill is too low. For mission use, remote measurements provide the only reasonable method of obtaining current and accurate C_n^2 values. Predicting turbulence is not practical, because the length of time over which numerical models are accurate decreases as the size of the cells being modeled decrease [10]. For turbulence profiling, prediction would require grid spacing on the order of centimeters, which leads to accurate prediction time scales of a few seconds. Currently, C_n^2 can be statistically predicted from weather conditions, but the predictions have an uncertainty that is too large to be useful. Current measurement techniques like scintillometers and temperature probes are not practical for use in missions. This leaves remote sensing methods as the only practical way to measure turbulence profiles. Real-time remote measurement methods are the subject of recent research, [8] [7] and the motivation for this project.

Fiorino and others [8] [7] were able to use clear-air weather radar returns to measure C_n^2 profiles. This provided a unique real-time, 3-D turbulence profiling capability. The real time, persistent, and remote measurements provided by the weather Radar returns has great advantages over conventional turbulence measurement techniques. The fidelity is much greater than using a statistically derived turbulence

energy distribution that is based on local weather conditions. At the same time, the use of these signals provides greater coverage than traditional methods including transmitter-to-receiver measurements done with laser or RF scintillometers, or thermal probes. However, weather radars have a few disadvantages: they can only detect turbulence in clear conditions, and they are limited in how often they take measurements. For the local NEXRAD radar in Wilmington, the scan time is a little over 9 minutes. Weather modeling can help to fill in part of this dwell period, but most of it will remain unknown. Finally, weather radar returns from clear air are of a relatively low intensity. This can reduce the range at which the radar can measure turbulence, leaving gaps in the area that is covered by radar. In Figure 1, plots of radar returns from the Wilmington Ohio Nexrad Radar are shown demonstrating varied coverage in an area.

These advantages and disadvantages of the weather radar method inspired this investigation. This work builds on the work of Fiorino and others by extending their method to scintillation measurements of cell-phone signals. This study suggests that measurements from cell-phone signals can augment the functionality of weather Radar: allowing C_n^2 to be measured in real time, wherever cell phone coverage is available, and during times of precipitation.

The cell phone method will not be able to provide the wide area coverage of a weather radar. Furthermore, there is not a historical backlog of measurements like weather radar. The expected benefits of using cell phone signals as opposed to weather radar returns comes from the wide coverage area of cell phone service, the constant availability of *base station* signals, and the weaker interaction of cell phone bands with precipitation. This leads to an extended coverage area, the ability to take continuous measurements in one location, and the ability to take measurements in all weather conditions.

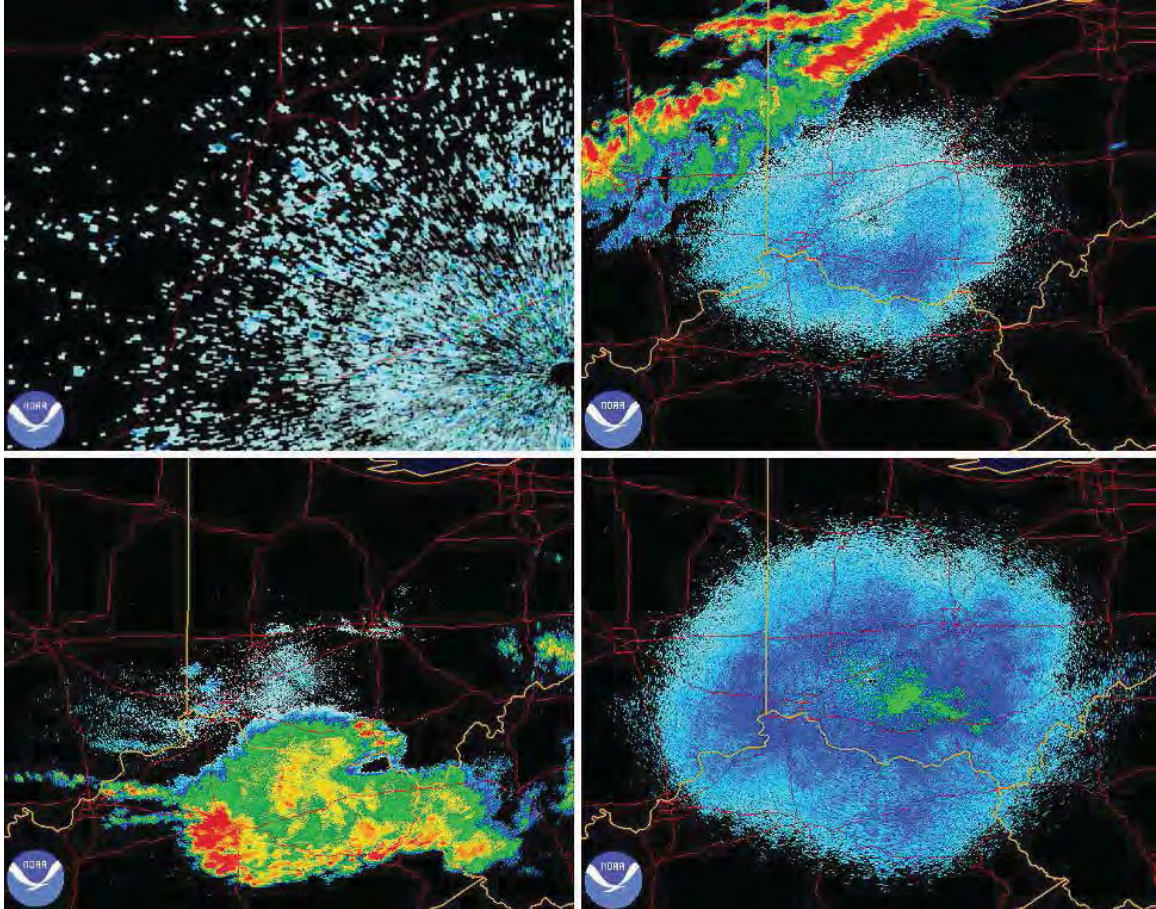


Figure 1. Four plots from the Wilmington Nexrad radar showing varied levels of clear air coverage. Clockwise from top left: Zoom of the Dayton area where measurements were taken with moderate coverage; Strong coverage with some range reduction due to the weather front; poor coverage that is possibly due to weather system to the south; Good coverage with long range.

Cell phone signals will provide a higher temporal resolution than radar, and multiple base stations may be used at once to provide a limited 3-D mapping of turbulence in an area. This provides a good synergy with the radar measurements. The radar measurements may be used to develop methods for extrapolating turbulence distributions in an area based on cell phone measurements of C_n^2 over several paths. By combining the two sensing methods, a persistently updated 3-D map of turbulence in

an area may be maintained.

In some cases, the returns from turbulence are relatively weak and may limit the range of the radar method. Wide availability of cell phone signals will allow for measurements to be taken in areas that are too far from weather radar stations to use Fiorino's method, or in situations where turbulence returns are masked by returns off precipitation. As an added benefit, this would be the first passive method for sensing C_n^2 known to the author. This could be important in situations where stealth is required. Furthermore, the method is expected to be cost effective, with an initial implementation done using data collection software running on a commercial Android® phone. Improved measurement methods are expected to be possible with purpose built hardware. The cost of this hardware is expected to be low because of the strong commercial development of RF equipment in cell phone bands.

II. Theoretical Background

Turbulence and Structure Functions

Stating that we are 'measuring' turbulence is used for the sake of simplicity, but the radar and phone measurement methods and how they react to the state of turbulence is important for understanding how measurements should relate. Many dimensions of the turbulence could be measured. What we are looking for is a description of how strongly the turbulence will effect EM propagation. For a measurement, it is often convenient to describe the interaction with a single number. Turbulence, in this case will be described by how strongly it changes the power and phase of EM waves after propagating a known distance. The single number that will be used is called a *structure constant*. A short introduction to turbulence is presented. This is then used to develop the concept of structure constants, and how they relate to *scintillation*. The following sections of this chapter will explore what is presented here, but in more depth. For a more detailed explanation of these concepts there are many good works on atmospheric turbulence and scintillation. For atmospheric turbulence, Robert Brown's book is a good source. [3] Tatarskii's report on turbulence and scintillation provides an excellent development of structure functions and energy distributions used to model turbulence. [15] Ishimaru's book on scattering by random media is an excellent source for information on scintillation and its relationship to turbulence power spectrums. [9]

In Fluid Mechanics of the Atmosphere Robert Brown defines turbulence as "the term for fluid flow wherein the path of an individual parcel of fluid is random, and thus unpredictable." This definition is good in that it captures two important points that will lead us to structure functions: turbulence is a type of fluid flow, and turbulence is random or unpredictable. Because turbulence is a fluid flow, it should be possible

to describe the flow using characteristics that are common to all flows. Since our measurements are based on EM propagation, it is worthwhile to identify the fluid flow characteristics that will effect the EM response of the air that the waves propagate through. Since this work is concerned with power measurements, Doppler effects caused by flow velocities will be ignored. This leaves the effects of bending, slowing, and scattering of EM waves. These are all caused by spatial and changes in the index of refraction along the propagation path of the wave.

The power of the waves at a receiver depends on how strongly the waves are scattered, focused, and defocused as they propagate along their path. All of these processes are a result of changes in the index of refraction that the wave encounters as it propagates. The index of refraction variation depends on variations in temperature, pressure, and composition. In a turbulent flow, the motion causes these properties to vary from point to point and over time. Scintillation at the receiver is thus dependent on variations in the refractive index induced by turbulence. Stronger turbulence results in greater variation in the index of refraction which lead to bigger fluctuations in power.

The spatial variation is unpredictable and is a defining characteristic of a turbulent flow. However, the structure is not an evenly distributed random variation about some mean value. There is a characteristic structure and shape to turbulent flows. Turbulence is characterized by whorls of varying size and random placement. An example of turbulent structure is presented in Figure 2. For turbulent gasses the motion of the whorl causes a centrifugal force that compresses air near the outer edge, and rarefies the center. The speed of the process causes the pressure changes of a given parcel to be approximately adiabatic. This leads to large scale gradients of pressure, temperature, and humidity across the whorl. These gradients manifest themselves as gradients in the index of refraction.

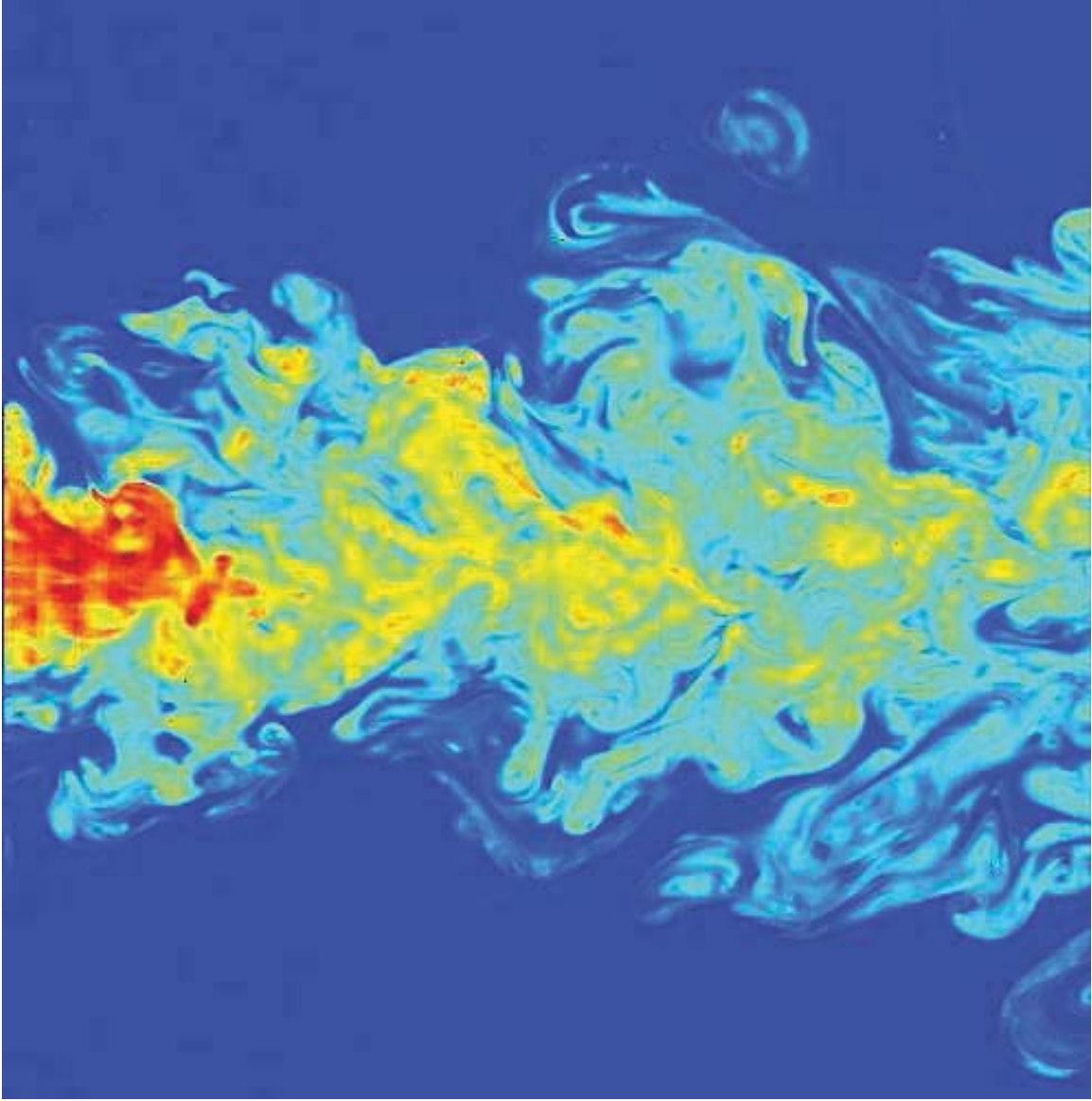


Figure 2. False color image of turbulence induced by a submerged jet made visible by laser induced fluorescence. The image is owned by C. Fukushima and J. Westerweel, Technical University of Delft, The Netherlands, and is used without permission or endorsement of this work under the Creative Commons license.

For variations in the index of refraction, the largest eddies behave like lenses: focusing the radiation. Smaller eddies disrupt the phase front of plane waves, causing defocusing effects similar to imperfections in lenses. All sizes of whorls scatter radi-

ation as well. For turbulence these optical effects depend on spatial changes in the index of refraction. For this reason the average index has no effect on scintillation, and has little meaning. Instead, the average variation, or gradient, in the index of refraction is the quantity that is measured. The structure constant used to describe the average strength of index variation is C_n^2 .

Turbulence in the Planetary Boundary Layer

In fluid mechanics the Reynolds number is used to help characterize the likely nature of a flow. Turbulent eddies will arise in fluids when the Reynolds number exceeds some critical value. This number is a dimensionless number given by

$$Re = \frac{VL}{\nu} \quad (1)$$

where V is the velocity of the fluid, L is a characteristic length, and ν is the viscosity of the fluid. This equation captures the fact that turbulence depends on the energy and geometry of a fluid flow and the viscosity of the fluid involved. Viscosity depends on many physical parameters of the fluid, but for purposes of *boundary layer* dynamics, we will consider it to be a constant. From this equation it can be seen that if the viscosity and wind speed are held constant, then turbulent motion will form past some characteristic length. The formation of turbulence has to do with the sheer stress created by changes in velocity within a given space. For fluid motion across a surface, the characteristic length assures that a flow will become turbulent once it has passed a given distance. The Earth's surface is a rough and complicated surface, with air flows being continuously driven from many sources. The low viscosity of air, $\nu \approx 15 \times 10^{-6} m^2/s$, leads to short characteristic lengths. Even without other wind sources, the diurnal heating and cooling of the Earth's surface creates enough vertical

motion to ensure that a region of constant turbulence exists.

This region of turbulent motion near a surface is called the boundary layer. In the case of the flow of the atmosphere over the Earth's surface the boundary layer comprises the region extending from the ground level to a height that is typically between 500 m and 3,000 m [3] [10]. Within this layer eddies range in size from being as large as the height above ground all the way down to a smallest scale which is typically on the order of a centimeter. [9] Within an eddy, the air swirls create a localized gradient of the index of refraction. In addition to this index variation from turbulence, there is vertical gradient in the index of refraction. This is caused by the exponential decay of pressure with height induced by gravity. The vertical index gradient results in a vertical stratification of C_n^2 .

In the case of boundary layer wind, the largest whorls are roughly as big as the height above ground level. This dimension is referred to as the outer scale of the turbulence [15], and is commonly denoted by L_0 . The turbulent motion leads to constant advection of air within the boundary layer. This advective motion mixes the air well and creates fairly constant *water mixing ratio* and *potential temperature* at all heights of the layer. The advection of air by the turbulence also causes the *absolute temperature* and *relative humidity* of the air to change as it moves through regions of varying pressure. Since the index of refraction of air is a function of the density and humidity, the variations in density and *relative humidity* become spatial and temporal variations in the index of refraction [15].

A dynamics theory of fluids in the regime of very high Reynolds numbers was developed by Kolmogorov in 1941. Kolmogorov's theory showed good agreement with observation and subsequently became the basis for turbulence theory in the boundary layer. [15] Kolmogorov's theory states that, in the regime of high Reynolds numbers, the rate of energy loss into heat for turbulent flows is much less than the amount of

kinetic energy within the eddy. Therefore, as an eddy breaks apart into smaller eddies, most of the kinetic energy of the system is transferred into the smaller eddies, with an insignificant portion becoming heat. As the eddy breaks apart, however, the scale length reduces, increasing the rate of heat dissipation. At some smallest dimension, l_0 , called the inner scale of the turbulence, the dissipation into heat begins to become appreciable. At this point the eddy losses to heat dominate as the eddy dissolves into the random motion of heat. Eddies whose size lies between the inner and outer scales are considered within the inertial subrange and are described by Kolmogorov's theory. Within this regime the statistical distribution of energy as a function of eddy size can be characterized with a turbulence spectrum. The spectrum of the turbulent energy can be approximately related to its interaction with waves by the C_n^2 constant.

Due to its chaotic nature, Turbulence is handled using statistical methods. It would be convenient if the average index of refraction, $\langle n \rangle$, and the variance of the index, σ_n^2 , could be defined. However, due to the nature of turbulence, these values, $\langle n \rangle$ and σ_n^2 , are themselves randomly varying in space and time. They can only be considered statistically homogeneous for such short times and distances, that these properties are not useful for our purposes. However, the statistical distribution of the difference in n as a function of separation, $n(\mathbf{r}) - n(\mathbf{r} + \Delta\mathbf{r})$ is approximately stationary for a large enough region, and for a long enough time span to be useful for describing the propagation of EM waves. [9]

A very good development of structure functions and constants for use in describing turbulence is given in appendices A & B of Ishimaru's book on propagation through random media. [9]. Based on this work, a brief summary of the motivation and meaning of the C_n^2 structure constant is presented here. This is included to help in understanding the measurement process.

In one dimension, the average change in n for a change in position, x is defined as

$$\langle \Delta n(\Delta x) \rangle = \langle n(x) - n(x + \Delta x) \rangle. \quad (2)$$

Here Δx indicates a finite change in position x , $n(x)$ is the index of refraction as a function of position, and the $\langle \rangle$ indicates the expected value of the quantity in the brackets. From this definition of $\Delta n(\Delta x)$ we further require that $\langle \Delta n(\Delta x) \rangle$ is only a function of Δx . Furthermore we require that $\langle |\Delta n(\Delta x)|^2 \rangle$ is only a function of Δx . From this we can show that $\Delta n(\Delta x)$ has the form

$$\langle \Delta n(\Delta x) \rangle = c\Delta x. \quad (3)$$

This is shown in [9] by taking the derivative of (2) with respect to x . Since Δn only depends on Δx , the derivative is

$$\frac{dn}{dx} \langle n(x) - n(x + \Delta x) \rangle = \frac{dn}{dx} \langle n(x) \rangle - \frac{dn}{dx} \langle n(x + \Delta x) \rangle = 0. \quad (4)$$

From (4) it can be seen that $\frac{dn}{dx} \langle n(x) \rangle$ must be constant, so $\langle n(x) \rangle$ has the form $\langle n(x) \rangle = cn + b$. This leads to

$$\frac{dn}{dx} \langle n(x) \rangle - \frac{dn}{dx} \langle n(x + \Delta x) \rangle = cn - c(n + \Delta x) = -c\Delta x, \quad (5)$$

and since c is an unknown constant, the negative sign on the RHS can be ignored. The constant in this equation is known as a structure constant for the variation of $\Delta n(\Delta x)$. So, structure constants describe how strongly a parameter is expected to change with a given change in distance, or time. Changes in the index of refraction are slow enough to be considered static for EM waves. C_n thus describes the average variation in n with respect to a change in position.

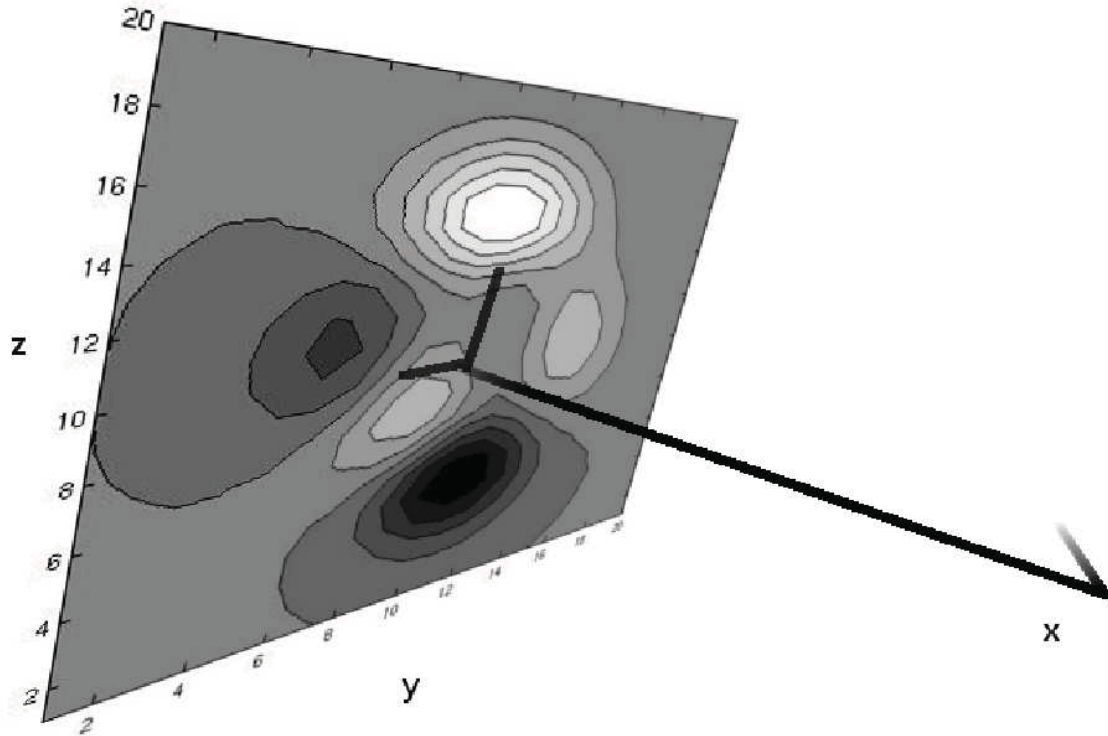


Figure 3. Cartoon of index variance in plane transverse to the direction of propagation.

The reason that the C_n constant is typically squared is because of the way that EM propagation is modeled. The variation of n in the plane that is transverse to the direction of propagation is important for determining the geometric optical properties of the medium. A good comparison can be made to the optical properties of fiber optics or laser gain medium. In these mediums the index also varies with position. For a derivation of optical properties of fiber optics and laser cavities see section 2.12 of Verdeyen's book on lasers. [16] The important concept to be gained from Verdeyen's examples is that the variation of the index of refraction in the plane that is perpendicular to propagation causes focusing of radiation, as if the radiation had passed through a lens. The equivalent 'lens' is a function of the length of the optic, and the structure of the variation of the index of refraction. However, focusing does not depend on variations in the direction of propagation. In Figure 3, the direction

of propagation is depicted along with the plane where variation is important. The C_n constants for both perpendicular dimensions end up multiplied together, leading to C_n^2 . For development of scintillation in the next section, a paraxial approximation is assumed: that variation in the perpendicular plane is locally isotropic and homogeneous. This removes the need for covariance terms, and allows for the variance of n to be described identically in both dimensions of the plane perpendicular to propagation.

In three dimensions it is possible that the variation in n also depends on direction of displacement in addition to the distance displaced. However, within the boundary layer, the well-mixed nature of the air leads to the index variation being locally constant in the horizontal direction. In the vertical direction the index variation has a strong logarithmic signal due to the air pressure dependence on height. For this study, the practices of previous works will be followed and the vertical variation C_n^2 will be ignored. This approximation will not likely affect this work because measurements of the same path using different instruments are being compared. So, the gravitational variation should affect both measurements equally and be transparent in the results.

Refraction and Scintillation

The index of refraction structure has three effects on EM waves. The largest eddies act as lenses and are responsible for focusing of the radiation. In focusing effects, the refractive index variations follow the principals of geometric optics. The smaller eddies create *dispersive* effects which affect the coherence of wavefronts and limit the strength of the focusing by large eddies. Focusing effects are created by turbulent eddies whose scale is much larger than the size of the first Fresnel zone [2] given by

$$F = \sqrt{x\lambda}. \quad (6)$$

F is the length of the first Fresnel zone, x is half the distance from the transmitter to receiver, and λ is the wavelength of the EM wave. The largest eddies are typically on the order of the atmospheric *boundary layer* [9], and cell phone wavelengths used in this study are about 16 cm.

As with any optical system, the focusing strength of turbulence is inversely proportional to the ratio of the optic size and the wavelength. [1] For this reason scintillation from turbulence focusing is more pronounced for the short wavelengths of visible light and Infra-Red (IR) than for the relatively long wavelengths of RF systems. Most modern scintillometers for measuring turbulence use a laser or microwave source as the transmitter. Because the wavelengths used by cell phones are around 15,000 times longer than near-IR wavelengths, the cell phone scintillation effect is expected to be quite small compared to laser scintillation.

C_n^2 is measured by looking at fluctuations in the power received from a source. It is assumed that the power of the source is known, and the power at the receiver would be some known value if not for the effects of the turbulence. Radar power received is based on scattering and reflection off the turbulent eddies. It can be shown [1] that when an EM wave passes through a region with a variation in the index of refraction, that part or all of the energy will be redirected, depending on the geometry of the wave and the index variation. Radar measures the intensity of the EM wave that is reflected back to the radar by the turbulence. The amount of energy returned is related to the strength of the index variation, and thus the strength of the turbulence. Scintillometers are different in that they look at the portion of the wave that is transmitted by the medium. Typical scintillometers measure the power received over an aperture. The turbulence causes the power to vary as the eddies in the propagation path change shape and intensity. The strength of the power variation is used to predict the strength of the turbulence. The development of the

scintillation relationship used for these scintillometers has the approximation that the backscattering is negligible, and that $\lambda < l_0$. [9]

There are several differences in a cell phone scintillometer that may cause inaccuracy in its C_n^2 estimates. Cell phone wavelengths are about 16 cm, so the assumption that the wavelength is smaller than the eddies is true for part of the turbulent spectrum, but not all. The smallest eddies are much less than a cell phone wavelength, and so they are not likely to have significant effects on the cell-phone scintillometer. However, mid-scale eddies may introduce some additional effects like defocus near the receiver. By changing the index near the transmitter, larger eddies may alter the multi-path beam steering, causing additional scintillation. This effect is explored more in Appendix A.

There are likely to be significant scattering losses from the inner scale eddies, and the cell phone may receive energy from several paths at once. Despite these differences, the direct path refraction process will still cause fluctuations in the signal power, and focusing effects will still be present. The equations developed for optical scintillometers are primarily based on these processes. It was expected that since the processes they model should still be present for cell phone signals, that equation 7 may be able to extract the turbulence signal in cell phone scintillation. The high correlation when this equation was used suggests that this expectation was met. In fact, the scattering losses and multipath effects may have increased scintillation, which would explain the large C_n^2 values obtained.

Rayleigh scattering may be more prevalent for the cell phone band than radar. This is expected because more of the spectrum will be in the Rayleigh range for the cell band. This may induce stronger power loss as Rayleigh scattering sends energy back more strongly than Mie scattering. Despite the fact that scattering by near and sub-wavelength whorls is not captured in the optical scintillation equation, the

driving process of the scattering is still the same. For this reason, the trends of the measurement should still track well, even if the values are wrong. Comparison to radar measurements was expected to be good because the cell phone would experience scattering, just like the radar. Since the wavelengths are similar, it is expected that even if the turbulence spectrum at the inner scale is not Kolmogorov, the scattering scintillation in both devices will still correlate.

Scattering, focusing, and *dispersion* effects are expected to be experienced differently for the cell phone than it is for laser and IR scintillometers. Due to the spread-spectrum Code Division Multiple Access (CDMA) bandwidth sharing techniques, the cell phone may alias phase scintillation effects into power scintillation measurements. While a full study of how turbulence affects CDMA receivers is beyond this work, some hypotheses are presenting in Appendix A. Additionally, the dispersive effects experienced by the beam optics of traditional scintillometers are not expected to manifest in cell phone scintillometry. In traditional scintillometers, dispersion manifests as phase incoherence across the receiving aperture, creating peaks and nulls across a planar aperture. [13] These effects are averaged out by using a large receiving aperture. Their aperture is many times the wavelength being propagated, and their measurement period is much longer than the wave period. This leads to typical scintillometers being time and space averaging devices. The cell phone antenna is a sub-wavelength device, and the sampling period is at least twice the bandwidth in order to meet Nyquist sampling constraints. Because of this the cell phone does not average over space or time. This may cause increased fading due to mutual interference of the cell phone wave arriving along different paths. Also, frequency dependent phase variation will could cause shifts in the steering of the phased array and timing of the rake filter used in communication. This may cause variation in the paths that the phone receives from, and reduce the effectiveness of the rake filter.

Because the effects of boundary layer scintillation on CDMA signal power levels are not well understood, C_n^2 will be calculated using a standard scintillometer equation. It was not expected that this equation would be accurate, but that it would provide proper trend agreement with the weather radar. Equation 7 was taken from [2],

$$\sigma_1^2 = 1.23C_n^2 k^{7/6} x^{11/6}. \quad (7)$$

Here $k \approx 39.8m^{-1}$ is the angular wavenumber for the center of the cell phone band, approximately 1900 MHz; $x^{11/6}$ is the path distance, and σ_1^2 is the Rytov variance. For small scintillation, where $\sigma_1^2 \ll 1$, the Rytov variance is approximately equal to the scintillation index: $\sigma_1^2 \approx \sigma_I^2$. Even for strong turbulence, $C_n^2 = 10^{-8}$, the Rytov variance in the cell phone band is less than 0.04 for a 1 km path. The scintillation index is given as [2]

$$\sigma_I^2 = \frac{\langle I^2 \rangle - \langle I \rangle^2}{\langle I \rangle^2}. \quad (8)$$

Here, I is the signal intensity, and the angle brackets denote the ensemble average.

The nature of the signal presents several advantages and challenges to measuring C_n^2 . Cell phone bands are at lower frequencies than those typically used for turbulence measurements, leading to possible concerns about the Fresnel zone size. The CDMA band used in the study is roughly 600 MHz wide and centered around 1900 MHz with tower spacing of around 1 to 10 km [5]. This gives an variation in F , the Fresnel size of the first Fresnel Zone, of 8.7 to 46 meters for a receiver placed half-way between towers. This indicates that the F may be greater than the outer scale of the turbulence L_0 for long transit paths from tower to ground as in Figure 4. If measurements are taken in this regime, $F > L_0$, the phone optical response will not be likely to correlate to other turbulence measurements. Apparently, it will be important to avoid taking measurements close to the ground and over long paths, as

the predictions of turbulence may be invalid. This regime can be avoided by choosing the geometry so that the receiver is close to several towers or by elevating the receiver. In this study, measurements were taken along a 630 m path, leading to a first Fresnel zone of 9.6 meters. Based on observations of the path, the First Fresnel zone is clear.

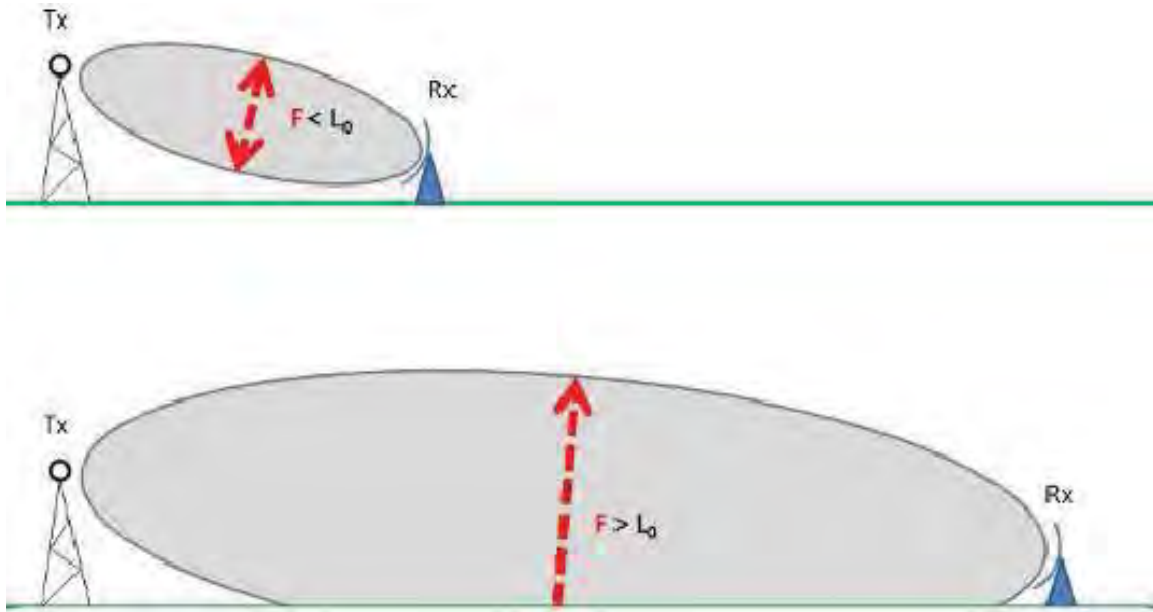


Figure 4. Above: A receiver that is close enough to a transmitter so that the Fresnel zone, F , is less than the scale height. Below: Moving the same receiver away from the transmitter causes the Fresnel zone to grow larger than the turbulence scale height.

In summary, the inner scale of turbulence is about 10x less than the wavelength involved, so the smallest eddies will act as random scatterers. As mentioned, the receiver's largest dimension (11.5 cm) is less than a wavelength, the de-phasing effects of the wavefront near a laser scintillometer's aperture are not expected to be present. However, multipath, and array phasing losses have not been investigated, and may contribute more to scintillation than is captured in the development of equation 7. However, the first Fresnel zone is easily clear of any obstructions, so the

focusing scintillation effects should be present. The process that may cause multipath scintillation is still tied to the turbulence power spectrum described by C_n^2 . This may partially explain the overestimates of C_n^2 predicted by the cell phone scintillation and the strong correlation of the trends in C_n^2 measurements taken by the phone and the radar. Hypotheses of the significance of these effects are presented as topics for further research in Chapter V.

Cell Phone Signal Characteristics

Measuring C_n^2 will make use of signal power levels received by an Android[®] phone using the Sprint[®] network. This section addresses some factors of cell phone design that will affect the phones ability to measure scintillation from turbulence.

Sprint uses CDMA in order to service accounts for both data and voice. While the specifics of CDMA are not the focus of this research, it is presented because of its importance to how the signal power is measured. CDMA is a spread-spectrum technique for dividing up the information capacity of an allotted band between multiple users. Spread-spectrum techniques are a class of channel capacity division techniques where every user makes continuous use of the entire frequency band to send and receive data. The resource division occurs by allotting portions of the total available signal power to each user. Synchronous CDMA is used for *base station* to phone communications and asynchronous CDMA is used for communications in the other direction [12]. The simpler synchronous method is outlined in some detail in Appendix A followed by a short summary on how this relates to measuring scintillation. Asynchronous CDMA is similar to synchronous, and the differences are not expected to be relevant to this work. In either form of CDMA, each user has a unique key that is used to encode their data. For an example consider a synchronous CDMA, 256 user cell. Each user gets a 256 bit key for encoding and decoding data transmitted from the base station

to the phone. In order to receive data, the phone must use its key to decode the signal it receives. The base station tells each user what key they will be using. The signal power the phone reports is the power of the signal after the decoding process has taken place. Because the signal must be decoded first, the phone may be susceptible to effects on the decoding process that conventional scintillometers ignore.

It is also important to note that a user's signal power is only part of the total power broadcast by each transmitter. The user's signal is summed with all of the other signals that the base station is broadcasting. The base station can vary the portion of the power that each user is allotted, and the number of users sharing the same power can vary dynamically. This may lead to short term scintillation in the user's signal power. However, these variations are likely to be on the order of the users bit rate, in the sub-millisecond regime. This scintillation is expected to average out by the relatively long, 1 Hz power measurement frequency. The base station output power may vary as well. Since the power levels were not available, these fluctuations are not accounted for. However, the high correlation suggests that base-station power variation is not severe or occurs at a dissimilar rate from turbulence scintillation.

The base station uses a rake filter in order to make use of multiple transmit paths. This filter allows for the signal to arrive along several paths, and thus be influenced by turbulence from different locations. The filter is similar in principal to the method of steering a phased array, but the filter is applied in pre-processing of each user's signal. The phasing in the rake filter is based on the lags and relative strengths of cross-correlation peaks in the signal being returned from the phone. Each base station sends out an identification and synchronization signal that is used by users in the base-station's cell to set their phone's transmitter strength, reception gain, and some of their encoding and decoding parameters. When a user is far from the tower, the phone will increase its transmitter power, lower its receiver attenuation, and increase

the number of codes that are used to send each bit. The last two adjustments may make the received signal power appear larger, without increasing the EM field amplitude of the signal. C_n^2 measurements assume that the signal power is constant except for variations caused by turbulence. Changes in the receiver gain or transmitter partitioning of signal power will affect the C_n^2 value. Obviously, any of these adjustments by the phone, which are not tracked, will cause errors in C_n^2 measurements. However, like the power variations done by the tower, the phone's power adjustments are on the sub-second scale, and the trends that are being investigated are on larger time scales. For this reason, small and fast adjustments may average out and not severely effect the correlation of recorded data to C_n^2 changes. The effects of these signal adjustments can be minimized because the greatest non-turbulence changes in strength are the free-space path loss and multi-path fading. Changes from both of these effects should be reduced by keeping the phone stationary.

A problem that turbulence may cause for digital signals is that it may distort the phase and power of the various frequency components differently. This will lead to *dispersion* in the signal, and cause some of the power of the signal to be lost. This is because the signal power is based on the peak correlation of the received signal and the users key. Varying the phase and amplitude of the signal's frequency components will, in most cases, reduce the correlation of the signals. Estimating these effects can be done more easily in the frequency domain. The codes used for encoding user data that is received from the base station are a set of $N = 4^m$ orthogonal binary sequences known as Walsh codes (m is an integer). These codes are mixed with data to be sent as well as encoding strings and random noise intended to smooth out the power in the signal, reducing bursts that the digital data may create. When the phone is not in use, information about the cell, traffic, and other information is being sent via specific Walsh codes in order to keep the phone updated. These codes are what is typically

being read to determine the signal power. An example of how the combination of phase and frequency scintillation within the band can provide variation in the average power of a processed signal is demonstrated in Appendix A.

CDMA is used by Sprint® and Verizon®, and some Asian carriers. The other leading cell-technology, GSM, is used by most European carriers, as well as AT&T® and T-Mobile®. GSM uses a form of channel resource allocation where each user is given a portion of the spectrum to use for communication. GSM may be usable for measuring C_n^2 , but only CDMA was used in this study.

III. Experimental Design and Methods

Experiment Overview

This experiment has four major sections to it: measurement and data collection using the phone, measurement and data collection using the radar, calculation of C_n^2 from measurement sources, and finally comparing the results of both methods. Details of these topics, and a description of how they were accomplished are presented in the following sections. This section will present an overview of the experiment.

There are some conditions, which have not been accounted for, where the phone and radar measurements are not expected to correlate. These are when the radar and phone are measuring different paths, when the radar is measuring reflectivity from precipitation instead of turbulence, and when bugs in the phone's logging software causes too few data points to be present to calculate a proper power variance. The first condition could happen due to multipath and reflection, or motion of the phone. The other two can be detected by looking at local weather observations, and the condition of the phone's data. Correlations under these conditions were much lower, and the data subject to these conditions artificially reduced the correlation of the measurements. Despite this, the correlation of the data was still quite high.

No attempt has been made to remove most of the bad data caused by these conditions. Strong drops in the scintillation index caused by too few data points were removed from the phone data. These drops created spikes in the phone's C_n^2 data. The spikes would be several orders of magnitude greater than other variations in the data. These values are considered to be system noise and their values are not representative of turbulence intensity. Since they significantly reduce correlation, and were easy to differentiate from normal data, these data points were removed before correlating the data. Correlations after removing these points was still high, no added value was seen

in spending time to remove the other effects. Surface weather observations from a nearby airport were downloaded for comparison with the C_n^2 data, and observations of the phone data logs were done for data sets that showed low correlation. These could explain most, but not all, of the remaining low correlation data sets.



Figure 5. Satellite image of Transmitter to Receiver path. The path length is 623 m. The distance from the KILN radar (not shown) is 42 km. Image copyright owned by ©Google 2011.

For this work, an ancillary goal was to make use of available resources, and not require the purchase of specialized equipment. Because of this, the phone that was used was not a dedicated measurement device, and measurement locations were restricted by the need for the phone to serve as a phone. In some cases, the phone may have been moving in a car, with the path location changing quickly. This may have caused some phone measurements to be spatially uncorrelated with radar measurements. A

single path had to be defined for each radar calculation. The path chosen is based on the phone and tower location stamps from a single measurement. The path is taken from a time close to when the weather radar file was recorded. In cases when the phone was traveling, the C_n^2 measurements are not expected to correlate to the associated radar measurement.

Even though the phone moved while taking some measurements, most measurements are from the same location. A satellite view of the path location is depicted in Figure 5. Notice that part of the path is obstructed by a neighboring house. This may have reduced signal correlation somewhat because the direct path passes through this structure. However, most of the path would likely be seeing the same turbulence that the radar sees.

It is assumed that the height of the transmitter above ground level is 50 meters, and that the phone is approximately 1 meter above ground level. Inaccuracies from this approximation are not significant. While the total path distance does affect the scaling of the C_n^2 measurement, the offset is linear. For this reason, when the normalized correlation of the phone measurements and radar measurements is taken, the path length error should fall away.

Taking Measurements With The Phone

Taking measurements with the phone was accomplished by writing an application that would record the power of the phone's signals, the date and time, the phone's location, and the location of the *base station*. The application was developed using the freely available Android[®] SDK. Once written, the application was used to log signal power levels. The recordings used in this test were taken from mid-June, until the end of August, 2011. Specifics of the application code are presented in Appendix B. Presented here are important factors that affect this work. These are hardware and

software limitations and uncertainties that are expected to affect the measurements.

Fortunately, despite the fact that cell phone was not designed to be a scintillometer, this work was able to use it as such. Sprint[®] was contacted about assisting in this work, but a response was not received. It was hoped that the transmitter power, and band use could be provided by Sprint, but work proceeded without this information. FCC information [5] [4] place a limitation of $\frac{40dBm}{4kHz}$ channel of ERP for PCS licenses. Sprint licensing in Dayton-Springfield includes a total of 50 MHz distributed over several bands. It is not known, however, how much bandwidth each base station is allocated, or what power the towers broadcast at. It is expected that the transmitter would be run at a lower power than the maximum allowed by FCC guidelines. This would be required in order to assure that no portion of the band goes over the $\frac{40dBm}{4kHz}$ power limit. Because the signal broadcast varies based on the user activity, power distribution over the band is likely to be uneven with transient power spikes throughout the band. In order to reduce interference between cells, adjacent cells should be given different bands to work within. [17] This leads to each cell having some portion of the band to work with so that CDMA codes can be recycled between cells. Sprint leases several bands in the Dayton-Springfield market. The lowest frequency license for Sprint PCS service is from 1865 - 1870 MHz, the highest is from 1990 - 1995 MHz. Their other licenses are distributed between these two, and add up to 50 MHz of total bandwidth. Not knowing the frequency center of the base station's transmit band will cause an offset in the calculated C_n^2 value. Bandwidth is not captured in the laser scintillometer equation 7, and its effects can generally be ignored. It may have a bearing on these measurements because of the CDMA decoding that precedes the power measurement. This is discussed further in Appendix A.

The phone reports power levels for two signals: voice and data. While these signals showed high correlation, they did not always behave the same way. in Chapter IV

it can be seen that power levels and C_n^2 values for each channel would sometimes disagree. Regardless of why the two signals disagreed, this shows that the cell phones are susceptible to some system induced noise in the signal power measurement. One certain source of noise is in the receiver attenuation and amplification. The device automatically adjusts these in order to improve the signal quality, but their status is not available. This noise will then propagate into the calculated C_n^2 values. These adjustments occur on a sub-second scale, so they may be averaged out to some degree.

It was expected that the Voice and Data signals pass through the same pre-conditioning network before being extracted from the received signal. This would mean that the attenuation settings for both signals are identical. For this reason it is expected that power changes would not affect the Voice and Data correlation. However, the Data and Voice correlation was worse than expected, sometimes much worse. For this reason it is theorized that these signals use different sub-bands, possibly different pre-processing hardware, or that the encoding keys do play a role in affecting the phone's power response to turbulence.

A significant source of cell phone signal fading is the multipath phenomenon. [17] In multipath fading, the signal power decreases because received signals arrive from different paths, often involving scattering, or reflection off of environmental features. These signals arrive out of phase with one another, leading to interference, and a varying signal power. This is quite different from a purpose-built scintillometer which receives its energy almost entirely from a single line-of-sight path. Cell phone transmitters use a 'rake' filter [12] which uses signal preprocessing and a multiple element array in order to steer much of the signal energy so that it arrives along the most favorable set of paths. Since the beam-steering is not known, the true path cannot be known. If the primary path deviates more than the turbulence coherence length [9] from the straight line path, then the scintillation detected will have little

correlation with the scintillation that should be seen for the straight line path. The turbulence coherence length is typically on the order of the first Fresnel zone or less. For this study the first Fresnel zone radius is about 10 m. While it is expected that most of the signal power arrives along the direct path, it is geometrically feasible for a reflected path to pass through turbulence beyond the 10 m coherence length.

Another effect that may be present for cell phone wavelength is that the smaller eddies may act as random scatterers. The smallest eddies are in the regime of Rayleigh scattering, $diameter \ll \lambda$, while slightly larger eddies are in the regime of Mie scattering. The Rayleigh scattering could lead to increased power loss in the phone's signal. The wavefront phase will also be distorted for cell phone signals. Since the rake filter is a signal phase steering method, the phase scintillation may cause disruptive beam steering. This may lead to increased multipath fading from strong turbulence. The intensity of multipath fading may also depend on the turbulence state along the various paths as well. The possible implications of these effects are the basis for further research suggested in Chapter V.

Ranked-correlation, and linear correlation functions are both included in case some of these signal distortion effects caused a non-linear response in the scintillation. The linear correlation was quite strong, so if any of these power loss processes are present, their effect on scintillation is likely to be linear with C_n^2 variation.

The resolution of the phone's power measurements is 1 dBm, and the calibration is uncertain. The antenna is not visible, and its radiation pattern is unknown. For this work it is assumed to be an isotropic receiver. The power reported by the phone is assumed to be the power after correlation of the received signal with the phone's key. This assumption is based on the large amount of band reuse in this spectrum, and a logical need to report the relevant power, not the noise power. The method of signal extraction is detailed in Appendix A. The signal processing relies

on a correlation function in order to pull the phone's communication channel out of the noise. For this reason, any propagation effects that would reduce the signal correlation will also reduce the signal power. This may make the phone sensitive to effects that are not detectable by traditional scintillometers. Specifically, if the phase of the various frequency components is changed, or the relative intensity of the frequency components is changed, then the correlation may drop down.

The logging software uses program functions provided in the Android SDK. This allowed for reasonable development times, but also limited the functionality of the device. It would have been preferred to record the power levels on a set time interval, perhaps every second, or half second. A good method for doing this was not found. Instead, the application opens a log, and records an entry every time the position or signal strength changes. For this reason the records are not evenly distributed. Some time periods have over 100 changes in a minute, others have less than 1 change every 5 minutes. Furthermore, the phone would sometimes close the log without notice, or stop taking measurements for extended periods of time. This lead to very few long-period measurements. Fortunately, the base station location, and local time is provided along with the power levels of both channels, and the phone's GPS location. This provides all of the information needed to estimate C_n^2 . Attempts were made to avoid moving the phone while measurements were taken. This was easiest to accomplish at night, which is why many of the logs begin in the evening and end in the morning.

Taking Measurement With The Radar

Radar measurements were taken from historical radar data recorded from the NEXRAD radar in Wilmington, Ohio. Radar sweeps take a little more than 9 minutes to complete, and it is not known when in the 9 minutes the measurements were taken. The method for calculating C_n^2 developed at the AFIT CDE by Dr. Fiorino and others [8] [7] requires extracting the average reflectivity of the radar bins that the path passes through. The method developed in the CDE experiments was not well suited to the automation required for this project. For this reason, a set of C libraries was developed that allows for the path averaged reflectivity to be calculated automatically. A detailed explanation of this code is provided in Appendix C. A short summary is presented here.

The libraries take a path and find the data *bins* in the radar file that the path passes through. In Figure 6 an example of a path passing through several bins is depicted. Each path endpoint is given as a latitude, longitude and a height above ground level. The radar file is opened, and the geometry of the *radar volume* is determined. The bins that the path passes through are determined. The percent of the path that passes through each bin is used to weight the reflectivity according to,

$$R_{average} = \sum_i \frac{l_i}{l_{path}} R_i. \quad (9)$$

Here $R_{average}$ is the path averaged reflectivity, l_i is the length of the path section that passes through the i^{th} bin, l_{path} is the total path length, and R_i is the reflectivity of the i^{th} bin.

A limitation of the radar sensing method is that data bins are sometimes missing for part or all of a path. This means that the average path reflectivity may not have any data at all, or is based on the reflectivity measured only in one small portion of

the path. The radar method uses the average path reflectivity to compute C_n^2 . This may not be the best method to provide correlation to scintillation measurements. Turbulence in the middle of the path has the strongest effect on scintillation, [13] and so scintillation based measurements will be more strongly influenced by turbulence in the middle of the path.

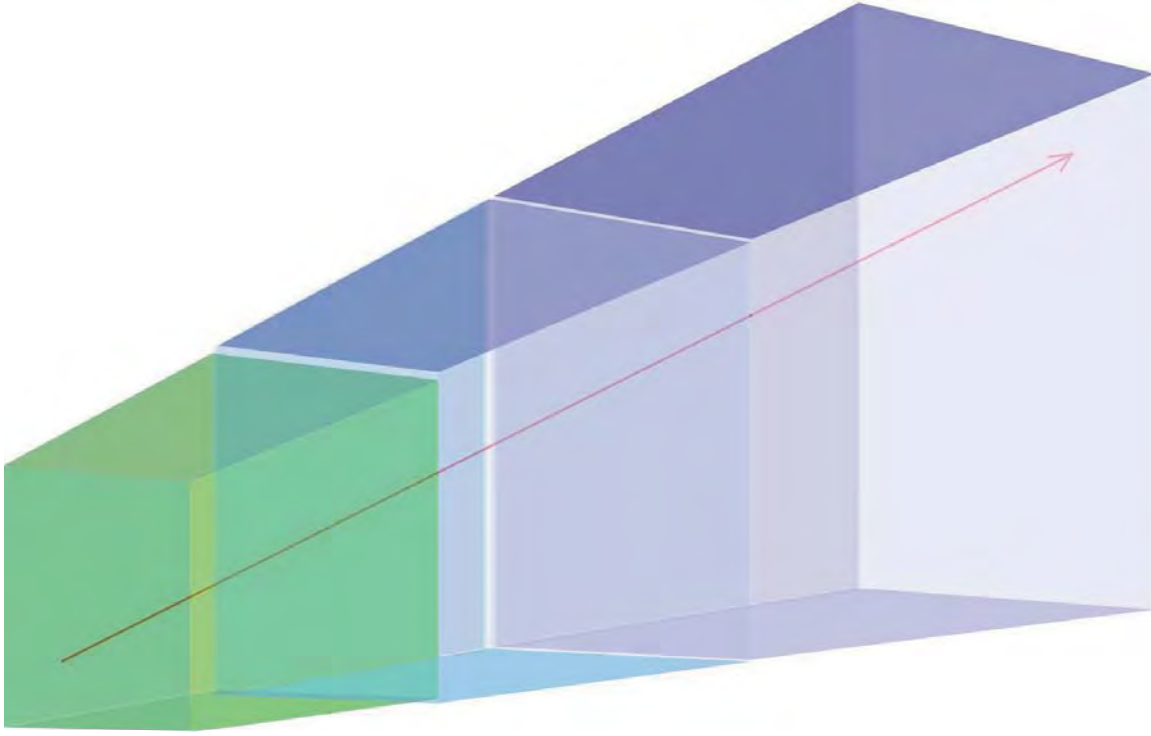


Figure 6. Cartoon of a path passing through three bins.

Another limitation of weather Radar is that the C_n^2 value is calculated from the reflectivity measurement, and precipitation also affects the reflectivity. The calculation method does not determine whether the reflectivity strength is from turbulence or water reflection. Because of this, precipitation will cause the radar to incorrectly measure strong turbulence profiles. Because most of this work was done during the summer, only a few of the measurements presented in the results involve precipitation.

Measurements from these times will not be expected to have a strong correlation to the phone measurements, but no attempt has been made to account for this in the results section.

Calculating and Comparing C_n^2 From Both Sources

Calculation of C_n^2 is done so that the radar and phone measurements can be easily compared. All of the steps listed below have been automated using a bash script that calls several custom programs. This section will follow the steps that the program takes after a phone data log is selected for comparison. Much of the comparison information is generated automatically and is included here. The next section outlines how the information from several logs was combined in order to determine the correlation of the method.

File Selection

In order to compare results, a phone data log is selected by the user. This data log defines the path, and the period over which the results will be compared. The time-stamp of the initial and final measurement are read and used to define the measurement period. Before anything else is done with the phone data, the radar files that will be needed are determined. Once the radar files are determined, C_n^2 is then calculated for each radar file.

Calculating C_n^2 From Weather Radar

Once the path-averaged reflectivity is determined, the average C_n^2 for the path is determined using

$$C_n^2 = 2.63\pi^5 \lambda^{-11/3} |K_w|^2 \frac{10^{dBz/10}}{1000^6}. \quad (10)$$

Here λ is the wavelength, K_w is the complex index of refraction for water at 5 deg C, and dBz is the path-averaged reflectivity. This is the equation given by Fiorino and others [7] for calculation without the wind speed correction outlined in their work. Correlation after the wind speed correction has not been investigated. The path used in the calculation is based on a phone measurement taken at nearly the same time that the radar file was recorded.

Calculating C_n^2 From Cell Phone Measurements

In order to easily compare cell phone measurements to the radar measurements, a cell phone data point is calculated for each radar data point. Equations 7 and 8 are used to estimate C_n^2 based on cell phone measurements. A C_n^2 value was calculated separately for the voice and the data line. Since the same methods were used in each line, power measurements will be referred to generically.

In order to determine the scintillation index, σ_1^2 , a time interval length must be chosen. Three interval sizes were tried: 30 seconds, 90 seconds, and 300 seconds. Each interval was centered on the time of the radar file time stamp. Because of the irregularity in the power measurement intervals, the number of data points in each interval is inconsistent. In general, shorter intervals showed more volatility and were more likely to be unable to calculate C_n^2 because they had $N < 2$ measurements in an interval (see Figure 7.) Because the 300 second intervals produced the greatest number of usable C_n^2 values, these plots were used for comparison to the radar measurements.

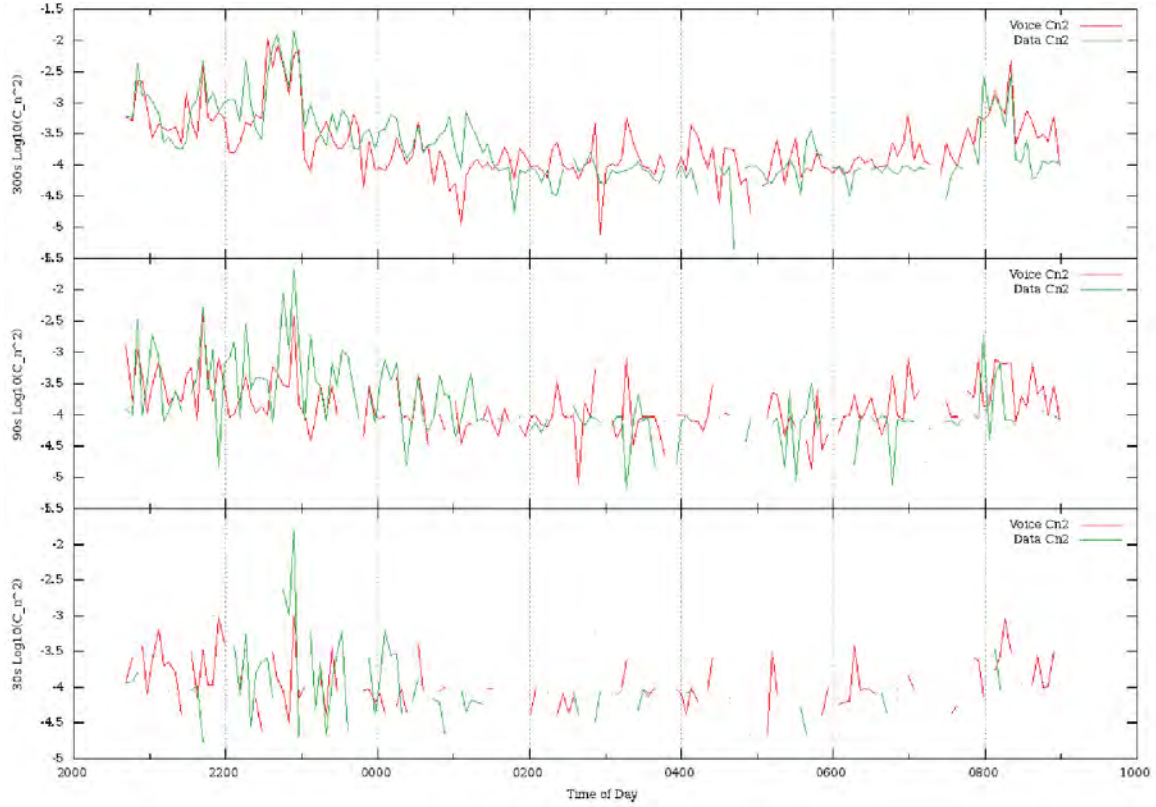


Figure 7. Three plots of C_n^2 Derived from cell phone signal power scintillation. The plots were each calculated from the same data set using different window sizes. From top to bottom, the window sizes are 300 s, 90 s, and 30 s. The data is from Monday, August 22, 8:37 pm EDT until August 23, 9:02 am.

For measurements where the number of data points, N , is at least 2, the scintillation index was calculated using equation 8. This is then used in Equation 7. After solving for C_n^2 it becomes

$$C_n^2 = \frac{\sigma_1^2 k^{6/7} x^{6/11}}{1.23}. \quad (11)$$

Here k is the wavenumber, and x is the path distance. For $N < 2$, C_n^2 is not determined.

For typical weather conditions C_n^2 values should vary from around $10^{-12} \leftrightarrow 10^{-16}$ [2]. However, measurements from the cell phone scintillation were in the range of $10^{-2} \leftrightarrow 10^{-5}$. This is due to the changes in power being much bigger than expected.

For typical turbulence, the predicted cell phone power scintillation is on the order of 0.1 dBm, but variations on the order of 1-10 dB were seen. Since the calibration appears to be wrong, the correlation function was used to look for similarity in the movement of the Radar measurements and the phone measurements. Investigations into the cause of unexpectedly strong scintillation were not carried out, but Chapter II and Appendix A present some theories that may explain the phenomena.

Automated Result Comparison

Through the rest of this work, three sources of C_n^2 data will be referenced: Radar, Voice and Data. For the sake of simplicity, these the C_n^2 measurements calculated from each of these sources will be referred to by the source name. The source names will remain capitalized whenever the C_n^2 data is referenced.

Once values of C_n^2 are calculated for all three sources; these values are recorded and passed to a plotting program. All plots have the local time in the 24 hour format EDT on the bottom axis. In addition to C_n^2 measurements, plots of the local solar zenith angles, and surface observations of wind speed are created. These results are passed to another program that handles plotting, and some of the comparisons. This program creates normalized versions of the data so that they can be plotted together, and does simple comparisons of the trend agreements. An example from a plot that showed high correlation is depicted in Figure 8

Initially, it was expected that the long term trends in the data would show the greatest agreement. However, this was not the case. It was noted, however, that the peaks and valleys of the various plots tended to agree. While the processing algorithms were being developed, a quick check for the high-frequency agreement was added to the calculation and plotting code. This provided the first evidence of correlation.

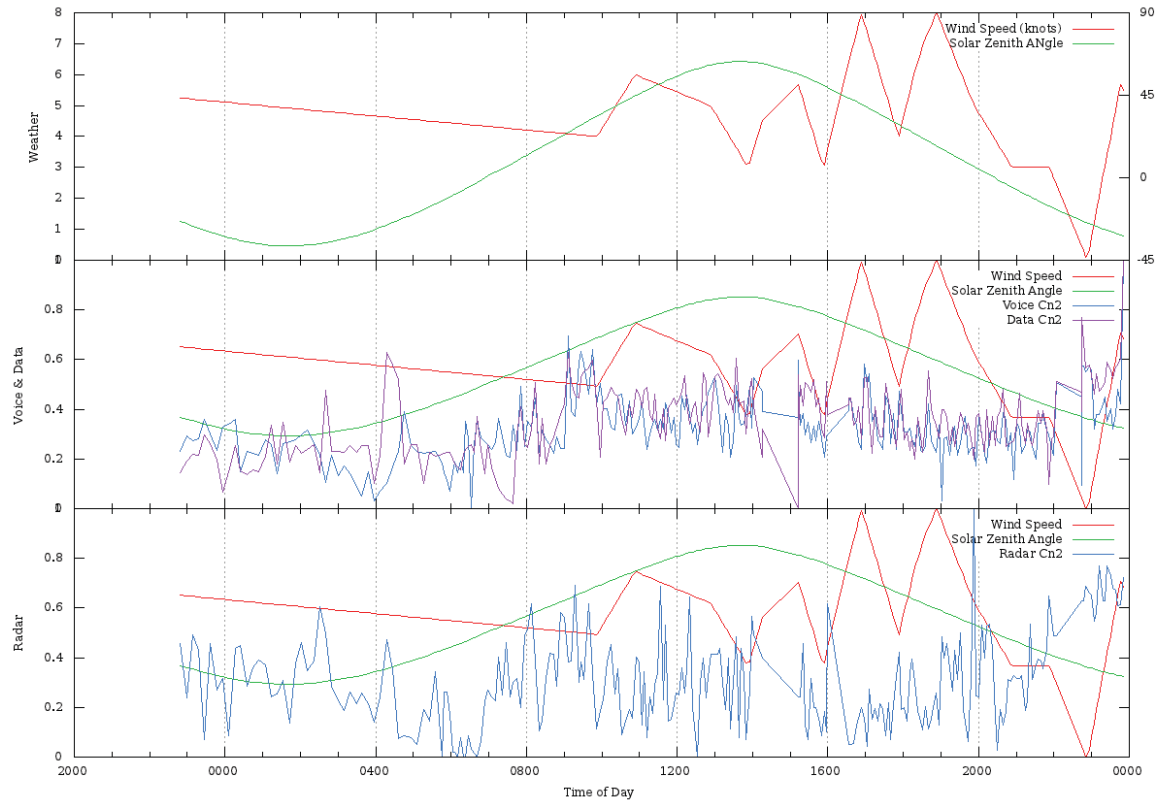


Figure 8. Top: Surface wind speed and solar elevation angle. Middle: Sun and wind data superimposed over normalized Voice and Data C_n^2 plots. Bottom: Sun and wind data superimposed over a normalized Radar C_n^2 plot. Time is local EDT, the plots begin August 17, 2011 at approximately 10:30 pm.

This normalization and comparison program created random data for null hypothesis comparison. This data allowed for a check to make sure the correlations of the plots is better than would be expected for correlations with random signals. More robust correlations would later be used when the data was ready to be imported into Matlab[®], but while testing the processing code, it was not desired to spend too much time coding correlation functions that were already available in Matlab.

Agreements between the data were compared using a high frequency ternary plot direction (increasing, decreasing, or constant) comparison. The function recorded the

change in direction from point to point, and assigned one of three values: -1, 0, 1. These values correspond to decreasing, no change, and increasing values. Similar to rank correlation, this method can pick out linear and some non-linear responses to common stimulus. A text file was generated for each data set showing how well the direction changes agreed, and what the statistically expected agreement would be for the data sets. The true data sets regularly showed better agreement than expected, while the random data did not.

Manual Comparison

In addition to the simple comparisons done within each data set, a more in-depth study of the trends over many data sets was done. The measurements from 42 data sets were imported into Matlab. Each set was comprised of phone, radar, time and weather data. Comparisons were done of each set, and of the ensemble of 42 sets.

The 42 largest (in bytes) data files were used to determine how well the measurement techniques agreed. These files covered all times of day, and were drawn from days between mid-June and late August, 2011. Each file covered between 6 to 14 hours. For each file, correlation measurements were made between the original C_n^2 data sets. Additionally, 112 sets of random C_n^2 data were generated from a continuous uniform distribution between -0.5 and 0.5. Each of the original data sets were tested against the random data sets. This was done to show the significance of the data correlations. The comparisons made are listed in table 1. In all cases the data values are shifted so that their mean is zero before the correlation tests are performed. Shifting the values was done so that statistical significance tests could be performed, and does not affect the results of the normalized correlation functions.

Table 1. List of Correlation Comparisons

Comparison Number	Data Set 1	Data Set 2
1	Radar	Voice
2	Radar	Data
3	Voice	Data
4	Radar	Random Plots
5	Voice	Random Plots
6	Data	Random Plots

After each of the 42 data sets had been processed, their correlation metrics were plotted along with representative metrics from the random data comparisons. In cases where the correlation between the true data is low, the original data was examined to see if there is a physical explanation for the low correlation. This led to some adjustments in initial method for calculating C_n^2 . It was noted that in some cases, either the Data or the Voice channel would record no changes, or no data within a given window. This would cause the C_n^2 data to have a few spikes with unrealistically small values. It is believed that these spikes are artifacts of the data collection and processing technique, and do not represent the turbulence intensity. For this reason, a routine was added that detects these spikes and removes them. The bad data points are replaced with values interpolated from the closest good data points.

Four different correlation tests were used in this study: cross-correlation, Pearson's correlation, Spearman's rank correlation, and Kendall's $\tau - b$ rank correlation. Cross-correlation was used for its ability to find similar signals in the data sets, and to find signals that may have delays in them. It is expected that the only signals that should be common to both the Radar and the phone measurements will be signals related to the RF propagation environment. The most significant effect in the fair weather afternoon boundary layer is Turbulence, [13] so correlation between the signals will be assumed to be based primarily on turbulence detection. The cross-correlation was expected to peak at zero lag for the turbulence signal. This happened often, but not

always. For this reason two cross-correlations were done. One at zero lag, and one with the customary lags from $1 - N$ to $N - 1$, with N being the number of data points in each measurement set. Lagged correlation is believed to be significant because the radar, and the phone may be affected by different parts of the turbulence spectrum, or by different aspects of the turbulence. Turbulence parameters are all related, but may react at different speeds to long term effects like the solar zenith angle and large scale weather changes. Inclusion of both may suggest some differences in what each method detects.

The Pearson and cross-correlation tests are linear correlation tests. They may not produce high correlations if the relationship between the data is non-linear. The Spearman and Kendall tests are ranked correlation tests. The ranked tests were included because they can detect non-linear monotonic relationships between the data. In this work, the Spearman correlation was a little higher, which is typical for these two tests. Both were included because in cases where their results are significantly different, these differences may provide insight into the relationships between the data.

The cross correlation was done to find the lag that produced peak correlation. The other tests were conducted at their traditional zero lag, and at the peak lag found by the cross correlation. The p value of the Pearson, Spearman, and Kendall correlation tests were used to check the statistical significance of the correlations, and to possibly detect a non-linear correlation between the data. Note that the traditional Pearson correlation is the same as the cross correlation at zero lag.

A p -test is applied to determine how significant the correlation values are. The p value is an estimate of the chance that the correlation value would happen for random data. If the p values are consistently low, then there is very little chance that the data accidentally correlated. Said another way, there is a good chance that the data

sets are related somehow. All p values are two sided because a high anti-correlation may be as significant as a high correlation. The inclusion of anti-correlation is due to a lack of understanding in the different processes relating the power measurements to turbulence.

All three correlation tests were carried out at the traditional zero lag. The tests were also taken at the lag that gave the peak in the cross-correlation. While this is not standard practice for these tests, it is believed to be applicable to this data. This is based on the fact that there may be linear and non-linear (but monotonic) processes occurring. If so, then the rank correlation tests may find significant correlation when the linear Pearson test did not. This produced mixed results which will be discussed in the following chapters. An attempt has not been made to take a sliding ranked correlation test in the same way a cross-correlation is a sliding Pearson correlation.

IV. Results

Correlation Results

Agreement between measurements is tested using correlation between the various C_n^2 plots. In all cases, the $\log_{10} C_n^2$ is actually used in the correlations. Correlations with randomly generated data is also done in order to have a comparison of the significance of the correlation. Linear correlation using Cross - correlation and Pearson's correlation showed the highest agreement between the plots. Perhaps more importantly, the Pearson p test showed a much higher significance than the ranked correlations in most of the tests. The rank correlation coefficients were lower and are included for completeness. However, most of the results will concentrate on the cross and Pearson correlations.

Cross Correlation

The cross correlation 'value' is the maximum value of the all the cross correlations taken at every possible lag. In all cases, the correlations are normalized so that the maximum autocorrelation of each signal is 1.0. The mean values of the data are removed before processing. As mentioned in the previous chapter, removal of the mean is not expected to cause error in the results. Removal of the mean turns the cross-correlation into a cross covariance, and allows for null hypothesis tests like the p -test for Pearson's correlation function. For the sake of simplicity, the tests will still be referred to as 'correlation' tests.

The absolute value of the correlation is considered the measure of similarity in the signal. See Figure 9 for an example cross correlation, it's absolute value, and the point that will be used as the maximum cross-correlation. The use of the absolute value treats correlation and anti-correlation as equally important. This may not be justified

because it is expected that the phone's C_n^2 should trend in the same direction as the radar. However, since the phone measurement method is not well understood yet, the anti-correlation strengths are compared with the correlation strengths. In the statistics this increases the likelihood of a high correlation, but decreases the significance of the correlation. Using the two-sided p test takes into account the inclusion of correlation and anti-correlation. Very few anti-correlation values ended up being the strongest points in the cross-correlation plots. This indicates that in most cases the two methods respond similarly to the underlying stimulus.

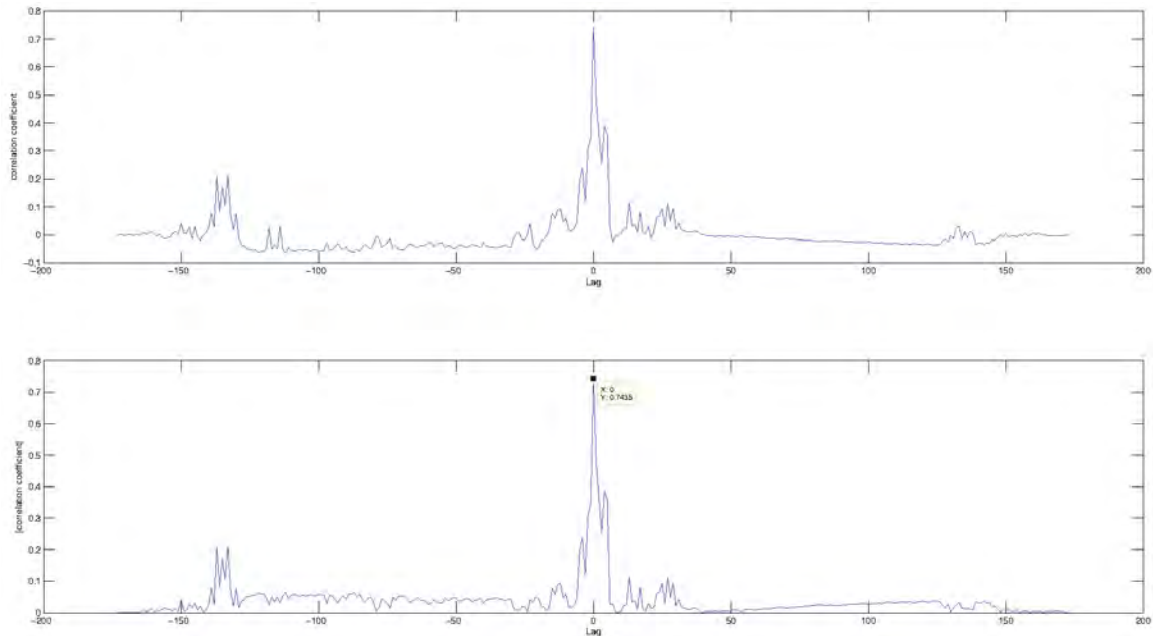


Figure 9. The top plot is an example cross-correlation. In the bottom plot, the absolute value of the correlation is taken, and the maximum value is picked out to be used as the cross-correlation for this data set.

The cross correlation is taken two ways. The first only considers the correlation values at zero lag. The second is the customary cross-correlation taken at lags from $-N + 1$ to $N - 1$, where N is the number of data points. For this study zero lag

is considered as: the true zero lag delay, or the lag with the phone shifted one step earlier. The zero-lag method is allowed to shift one measurement because the time of the radar measurement may vary within around 9 minutes of the file time stamp. This could lead to the phone measurements being aligned more closely with the radar measurements one time step earlier. The greater of the two correlations is used.

For the random data, the correlation coefficients are taken for all 112 random data sets. The mean of these maxima is then used as the 'random maximum',

$$Correlation_{random} = \frac{1}{N} \sum_i^N \max(R(x|x \in \mathbb{Z}, -n \leq x \leq n)) \quad (12)$$

Here R is the cross correlation function for any time shift, x . The use of a mean of 112 correlations is to ensure that a value for the random correlation is representative of how well random data will correlate. The mean ensures that it is very unlikely that the random correlation is unusually high or low.

Furthermore, the standard deviation of the random correlation values gives a measure of how significant the correlation of the true data is. If the correlation of true data is s standard deviations from the mean, then the chances that random data could produce a correlation or anti-correlation of this strength or more is equal to the area under the wings of the distribution past s standard deviations. This is the area p test attempts to estimate.

If the distribution of the coefficients is reasonably Gaussian, then there is little chance that a random correlation will be 3 or more standard deviations above the mean. The 112 point distributions looked reasonably Gaussian. As with most random processes, increasing the number of correlations showed the distributions looking more Gaussian. Little change was noticed in the mean or standard deviations of 112 points and the increased 1200 points, but the bell curve appearance is easier to see. In Figure 10, four distributions from correlations of random data to the Radar and Voice plots

are pictured. The top two plots are from zero lag correlations, while the bottom two plots are from normal cross-correlations. The skew in the lower plots is possibly due to the fact that all 1200 random data sets were compared to the same true data sets. In all cases, it seems reasonable to assume that the likelihood of a measurement being more than three standard deviations from the mean is low for these distributions. Next we shall show that the true data correlations were more than three standard deviations above the mean of the random data correlations.

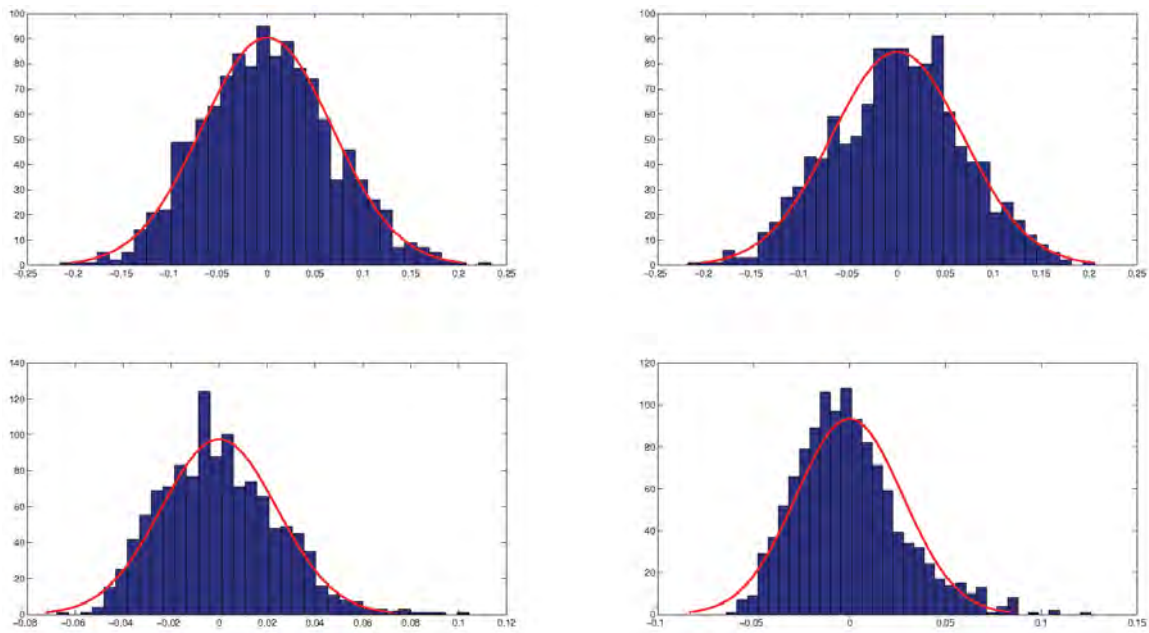


Figure 10. Four distributions of the measured correlation between 1200 sets of random data and C_n^2 measurements from Radar (Right Top and Right Bottom) and Voice (Left Top and Left Bottom). Normal distributions are superimposed in red.

In Figure 11 the averages of the correlations for the 42 data sets are presented. The left chart is the zero-lag correlation, and the right chart is the correlation taken at any lag. it can be seen that the correlation between the Data and Voice lines is high in both charts. This is expected as both measurements are done in a similar manner

with the same device. The large standard deviation of these measurements, and the fact that the correlation strength varies indicates that the correlation between Voice and Data may be dependent on other factors beyond turbulence. If the channels were sending similar signals in similar bands through the same environment with the same endpoints, then they should see similar variation. These unaccounted processes are likely to decrease correlation with the Radar data as well, but their effect is not quantified in this work.

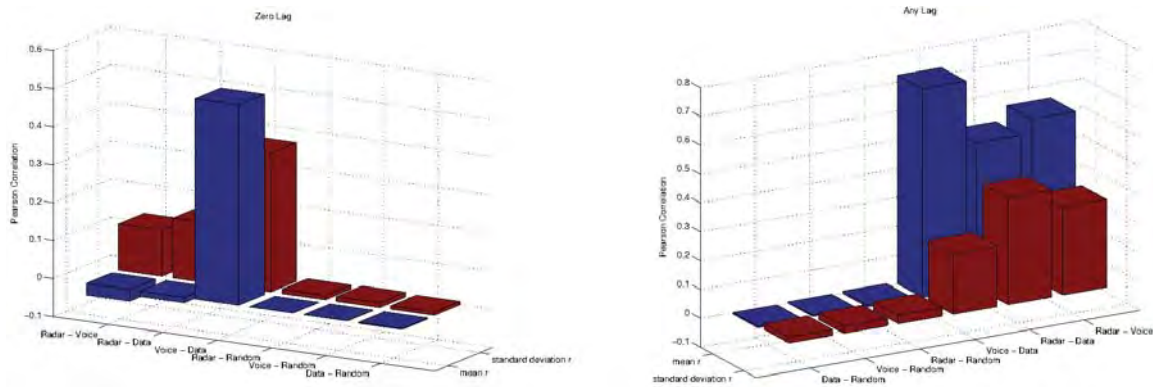


Figure 11. Left: Correlations of the various plots with any time lag. Right: The same correlations when with either 0 or -1 time lag.

In the plot from zero lag, the correlation between the Radar and phone measurements is only slightly larger than the correlation to the random signal. However, the correlation increases greatly when the time lag is allowed to extend to all possible values. These high correlations indicate that there are processes that both measurement methods are reacting to. The fact that the correlation peaks at varying lags can indicate that measurements are of the same signal but the times are out of synchronization. However the random variation from 0 to many hours of lag indicates that this is not the case. Another interpretation, is that the measurements are reacting to a common stimulus through different processes. This could be due to the difference

between the Radar taking a 5 second measurement in a 5-9 minute interval, and the phone averaging over 5 minutes with a similar interval. Possibly, the two methods are reacting to different parts of the turbulence spectrum, or the scattering and focusing power of turbulence respond at different rates to common stimuli.

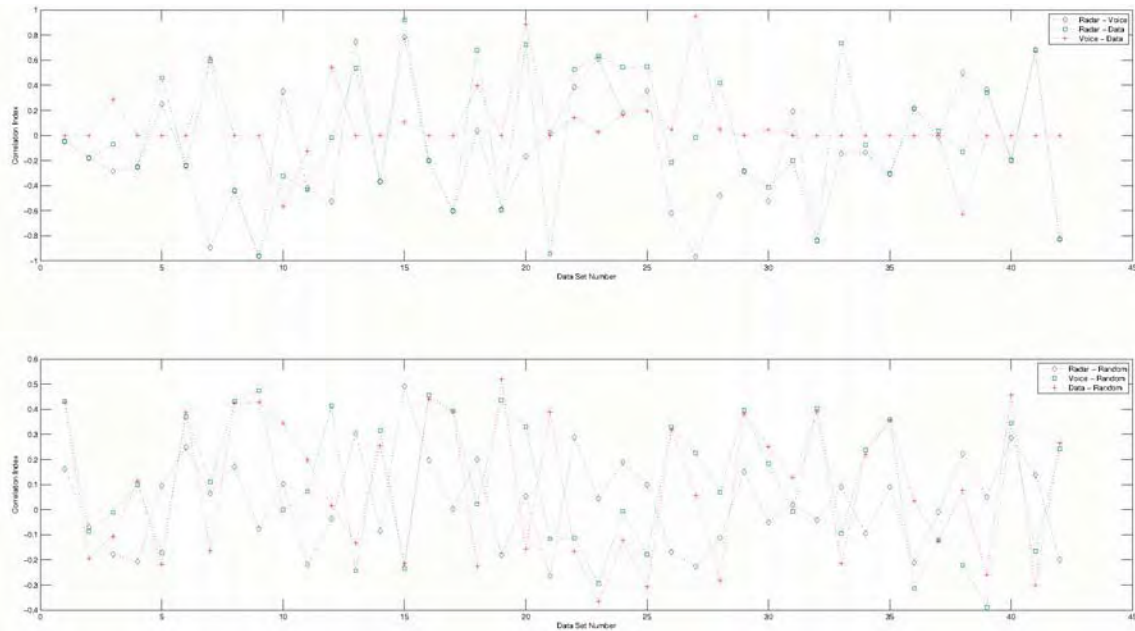


Figure 12. Lag at cross correlation peak. The lag values are normalized by dividing by the number of points.

Seeing that the correlation lag varied from data set to data set, an attempt was made to look for a relationship between the lag and measurement conditions. The lag values that gave the greatest correlation were plotted, and sorted by: the day of the year, the mean time of day of the data, and the number of points in the data. It initially appeared that plots that centered around the late morning had a tendency to peak at a greater lag shift. However, when the lag shifts were normalized, this trend went away. The normalized lags for each data set are shown in Figure 12. The trend of the larger lags for data centered on mid-to late morning probably was caused by the

fact that the files were most often started in the evening, so the longest files tended to have a mean collection time near the late morning. Since the largest shifts would have been associated with the data sets with the most points, this trend appeared. Within the normalized plots, no relationship or trend in the lag was apparent.

The lack of correlation between the Radar and Phone at zero lag was puzzling. Because of this, and the fact that the lag of the correlation peak was so random in the time domain, the cross-correlation plots were Fourier transformed into the frequency domain. There seemed to be more consistency in the frequency of correlation than in the time of correlation. These Cross-Power-Spectral-Density (CPSD) plots often showed a peak correlation period of about 500 seconds, and many showed another at about 100 second period. These peaks may indicate that the systems see different parts of the turbulence spectrum more effectively, and thus react to energy influx at different rates. A plot of the peak period of each CPSD is presented in Figure 13 below.

It is not surprising to note that the two measurements taken by the phone, Voice and Data, tended to correlate well at zero lag. The instances where the Data and Voice correlation peaked at a non-zero lag do not appear to relate to the strength of the correlation. Figure 14 and the left plot of Figure 11 do not provide convincing evidence of a relationship between the Radar measurements and the phone measurements. In these plots, none of the Radar to Data or Radar to Voice correlations show peaks that are nearly as high as the Voice - Data correlation. However, the agreement at any lag is good. This is interesting because it indicates that the phone (and the radar) are measuring turbulence but they may not be adequately characterizing the whole spectrum. Or that their measurements show part of the spectrum and disturbances from outside the Kolmogorov spectrum.

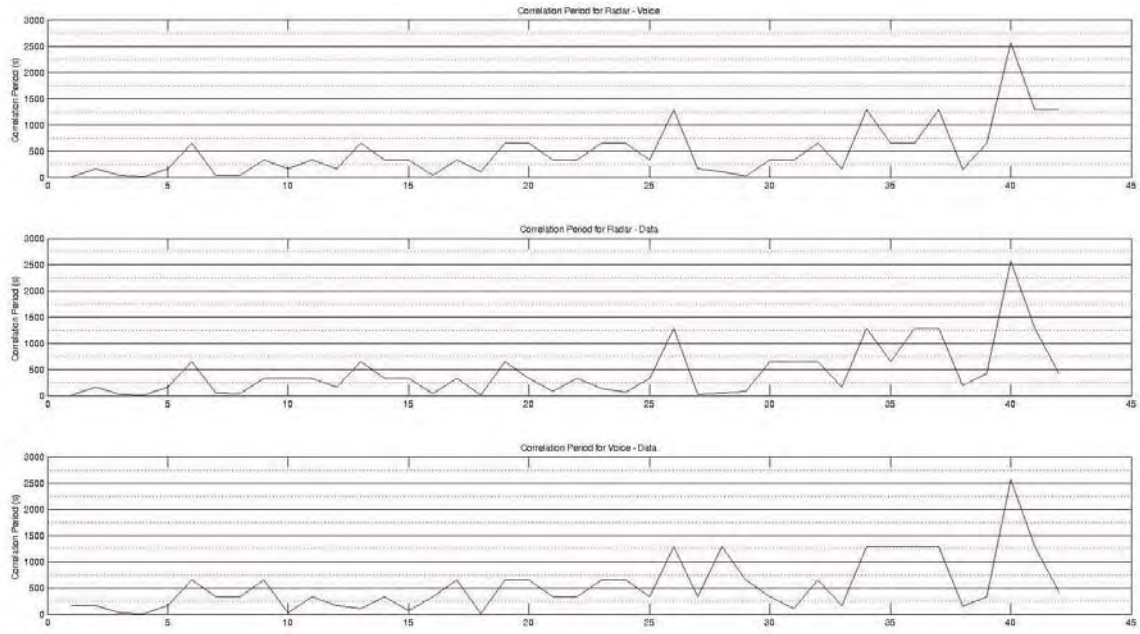


Figure 13. The peak correlation period in the CPSD of all 42 data sets.

The correlation of the random data sets with each of three measured sets is nearly the same, regardless of whether the random data was being correlated to Radar, Voice or Data measurements. This can be seen in the lower plots of Figures 14 and 15. This is expected for signals with no correlation, as the correlation pattern should not depend on what is in the measured signal.

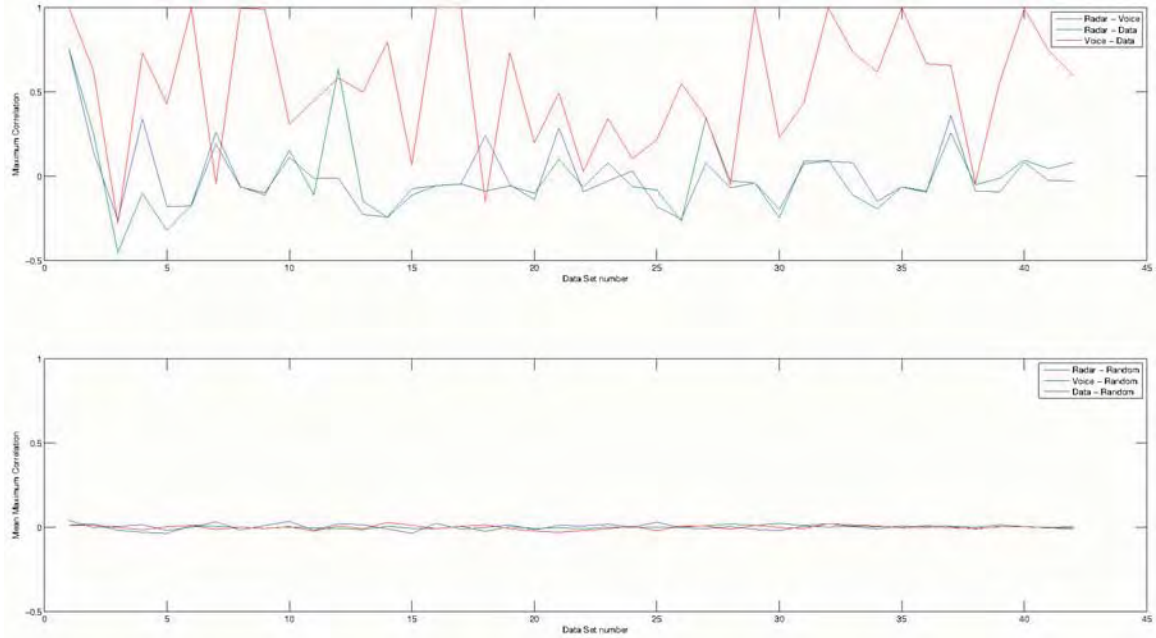


Figure 14. Top: The correlation coefficients for the three data sources are plotted. Bottom: The mean correlation coefficients of each data source and random data sets. All coefficients are normalized. Each of the three data sources was correlated with 112 random number sets. Values are taken from the zero-lag correlation, or the first set lags by 1 correlation: whichever is larger.

Although high, the Voice - Data correlation drops off dramatically in some points. A cause has not been found for why the two channels can agree very well at times, then not at all at other times. It is reasonable to assume that both channels are experiencing a similar propagation environment, as the endpoints are identical. Some other factor must be affecting their power level, or how the signal reacts to the environment. There are more low correlation points on the left side and center of the Voice-Data correlation plot. These plots tended to have fewer data points than the plots on the right.

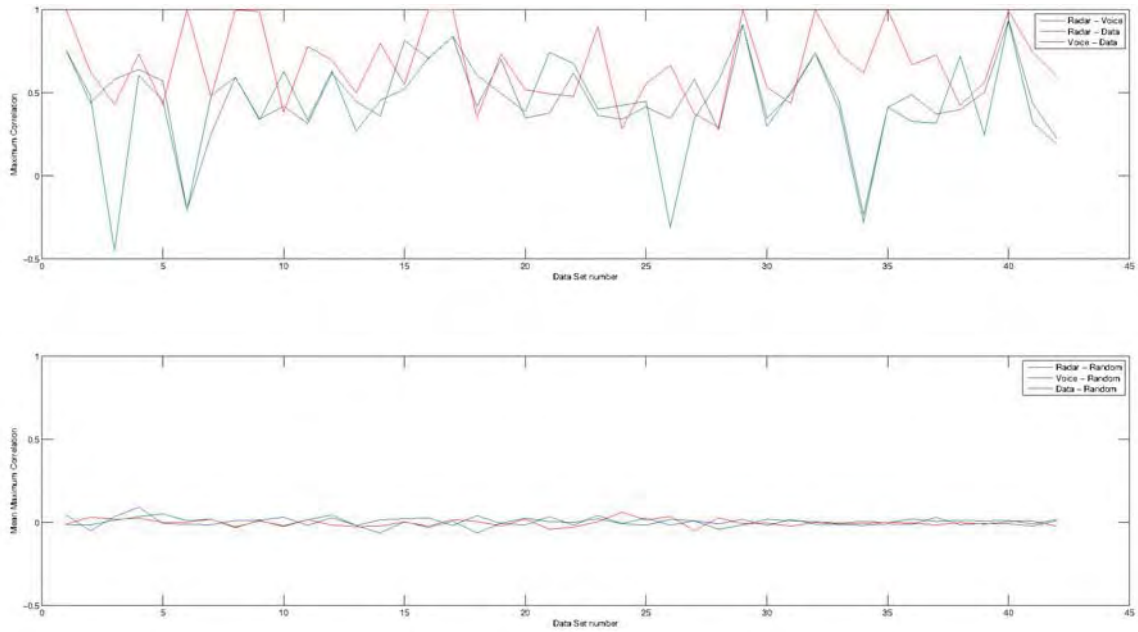


Figure 15. Top: The maximum correlation coefficients for the three data sources are plotted. **Bottom:** The mean maximum correlation coefficients of each data source and random data sets. All coefficients are normalized. Each of the three data sources was correlated with 112 random number sets. The maximum is compared to correlations at all possible lag values.

As depicted in the left plot of Figure 11, the average zero-lag-correlation between Voice and Data is 0.47, with a standard deviation of about 0.35. The large standard deviation is expected, because it indicates that the correlation is typically high, or low, with very few values in-between. Examining the Data and Voice C_n^2 plots for the lowest and highest values showed little obvious cause for the plots having low or high correlation at zero lag. Some of the plots had missing data points, but there did not seem to be a relationship between data loss, and the correlation. Some of the nearly perfectly correlated plots had missing data, and some of the nearly uncorrelated plots were missing data too.

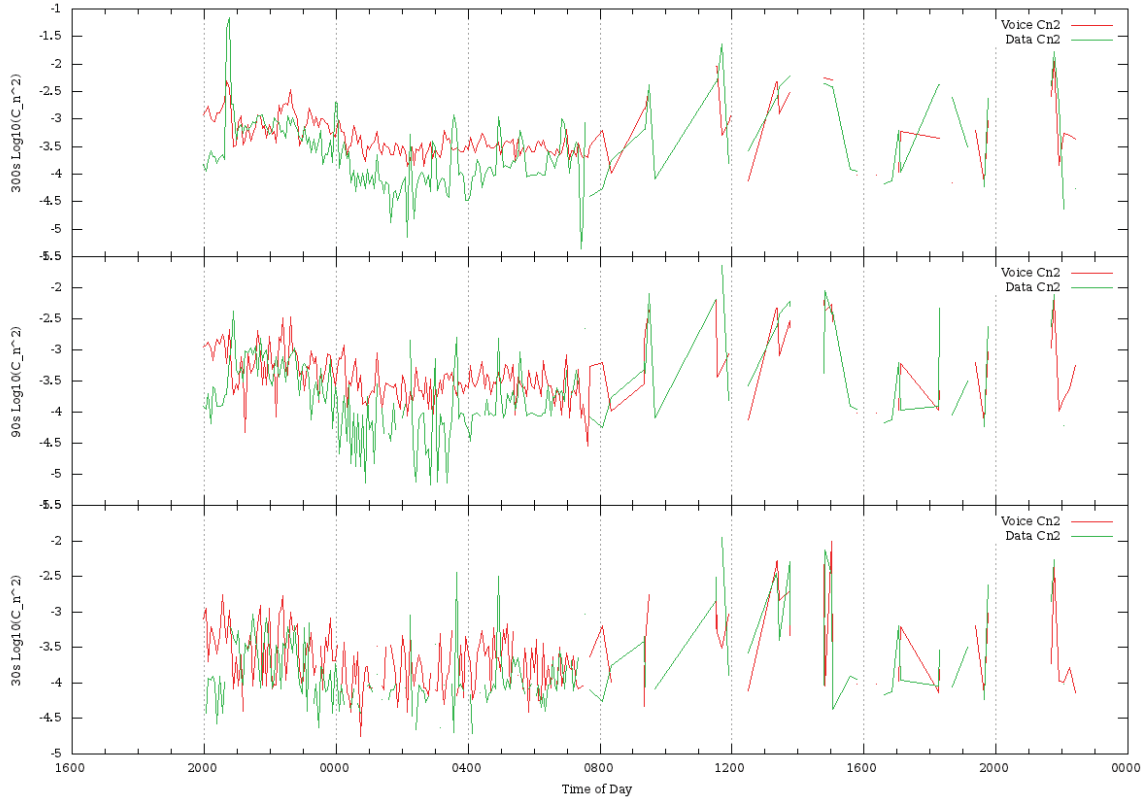


Figure 16. C_n^2 values from August 22 - 23. The second half of the plot shows many points where data was not available.

Loss of data in the plots can happen for several reasons. An example of this is pictured in Figure 16. In this case, the phone's data log skipped long periods of time near the end of the file. Some plots showed sections where C_n^2 dropped dramatically, probably due to insufficient data being present to calculate a meaningful σ_1 . This was compensated for using techniques described in the previous chapter. Another common cause was low reflectivity in the Radar. The processing of phone data is tied to Radar data points, so if the Radar was not able to measure a return, there will be missing data in the phone plot. In addition to data loss from scintillation below the detectable range of the phone, bugs in the logging software may prevent the phone from recording scintillation. Removal of suspicious data from the statistics

below may not always be justified, and it could mar the validity of the results. It is not known if the phone power wasn't changing because it wasn't being measured or recorded properly, or if the scintillation was actually quite low. Proper compensation would require a large investment of time and effort, and would not provide significantly 'better' results. Because of this, the removal of outlier peaks is the only compensation that was done.

When the full cross correlation is considered as in Figure 15 the Voice - Radar and Data - Radar correlations increase dramatically. The right plot in Figure 11 shows the results on the mean correlations. The Voice - Data correlation is still the highest. While the Data - Voice has increased, the standard deviation has decreased from 0.35 to 0.18. The plot of the correlations in Figure 15 has many of the same features as the plot in Figure 14. This shows that the limitation of zero lag may affect the total strength of the correlation, but signals that are weakly correlated at zero lag tend to be weakly correlated for all lag values. For the Radar - Voice and Radar - Data plots, there was often low zero-lag correlation. Also, the p tests from Pearson and the ranked correlations showed a low significance at zero lag. In most cases the zero-lag data was shown to be slightly anti-correlated.

Pearson, Spearman, and Kendall Correlations

This section will be devoted to comparing the Pearson, Spearman and Kendall correlations of the Radar - Voice, Radar - Data, and Voice - Data sets. Before going into these, a brief summary of the correlations with the random data sets will be presented. All three correlation tests produced nearly identical results in the random noise comparison. For the random data, all three tests will be referred to in the generic sense and plots of the Pearson correlation will be used to represent all three correlations.

All three of these correlation tests include a p-test. This number is used to indicate how significant the correlation is. The p-test can vary from 0 \leftrightarrow 1 Small p-test values indicate that the correlation value is significant, and large p-test values indicate that the correlation value is not significant. In all cases, the p-test value is the double-sided p-test computed using the 'corr' function in Matlab[®]. Based on the size of the data sets, the Kendall and Spearman p-tests will be calculated using approximations or permutations. The Pearson p-test is calculated using Student's t distribution, which is reasonably accurate assuming that the null hypothesis correlation distribution is Gaussian. As indicated in Figure 10, this is a reasonable approximation. An physical interpretation of the p-test is that it is a measure the null hypothesis. The null hypothesis testes how likely it is that random data with the same number of points would produce a given correlation value. The two-sided test accounts for anti-correlation, and correlation. A p-test of 1 only occurs for zero correlation, and a p-test of zero is impossible for finite populations.

Correlation with noise produced expected results: depicted in Figure 17. The correlations are low in all cases, and the p-values are high. This indicates that the tests are treating random data in an expected way, and if that the true data has a much higher correlation, then it is likely that the data sets are correlated.

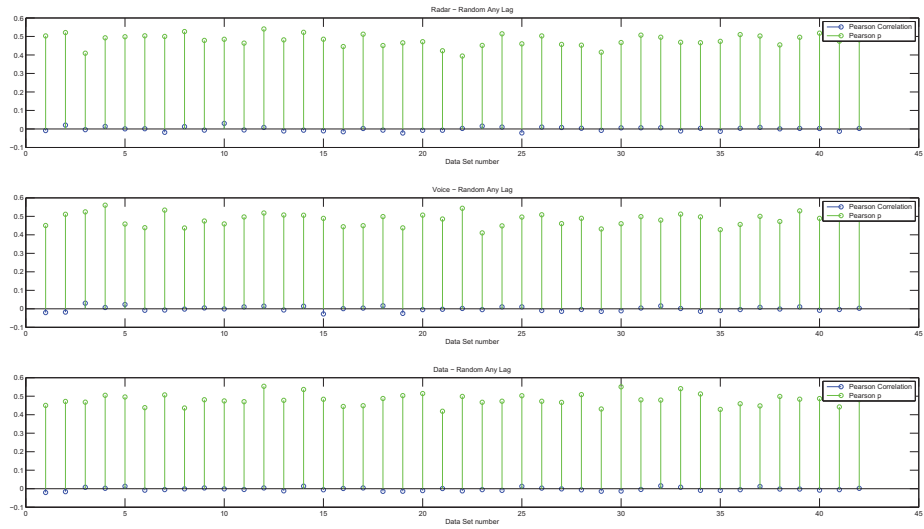


Figure 17. Pearson correlation of three C_n^2 data series to random data.

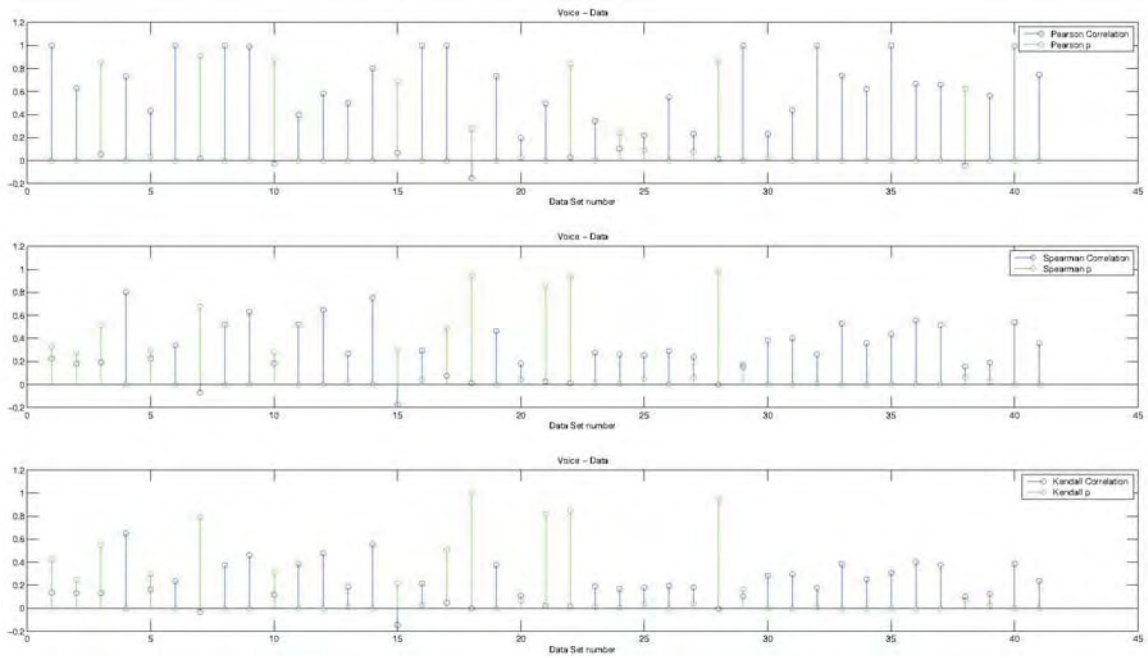


Figure 18. Correlation of Data and Voice measurements taken at zero lag.

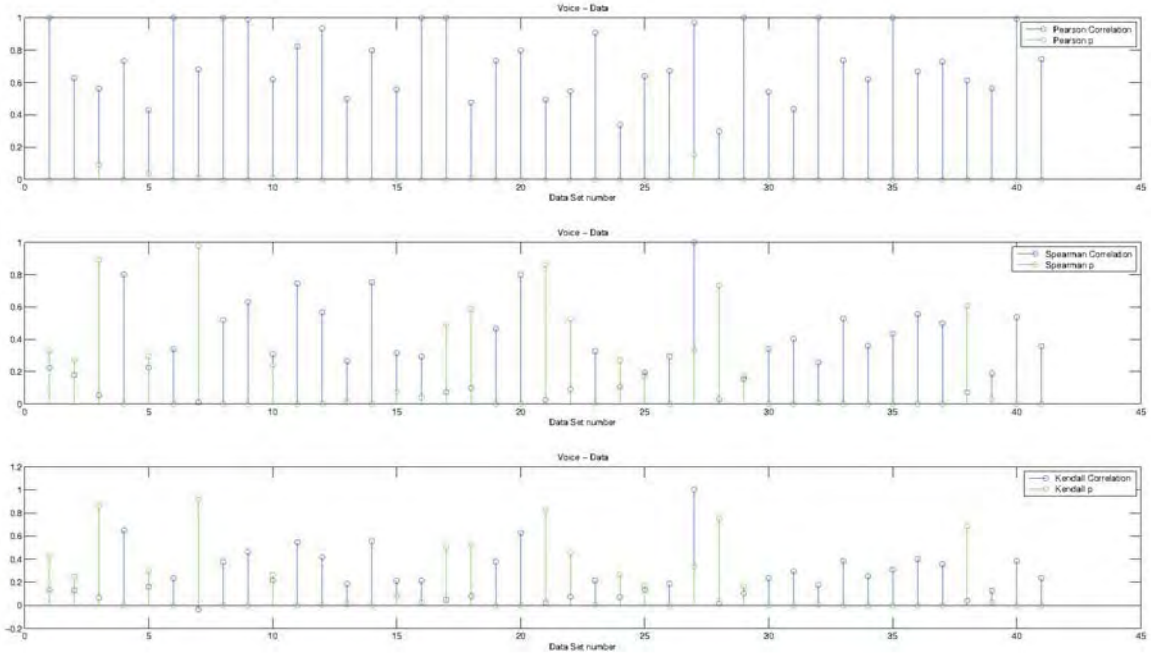


Figure 19. Correlation of Data and Voice measurements taken at the lag where the cross-correlation peaks.

The Data - Voice correlation is shown in Figures 18 and 19. Many of the cross-correlation peaks for this data are at zero lag already, which is why the zero-lag plot still has some strongly correlated data. The very high Pearson coefficients indicate that there is a strong linear relationship between measurements taken in both channels. In the zero lag plots, there are a few instances where the Kendall and Spearman coefficients show a stronger relationship than the Pearson. There are also several instances where the Pearson coefficient is much higher than the ranked coefficient. When the cross correlation lag is applied, the Pearson correlation becomes very strong. The ranked correlations also improve. The coefficients all show a positive correlation at this lag. This indicates that the Radar and Voice channels respond monotonically to the major processes that vary C_n^2 measurements.

The Radar - Voice and Radar - Data correlations are depicted in plots 20, 21, 22, and 23. The responses of the correlations in these plots is similar enough that

they will be discussed together. As in the Voice - Data correlations, the correlation improves strongly at the lag time suggested by the cross-correlation. The Pearson correlation is also much stronger than the ranked correlations. This suggests that the relationship between the Radar and Phone measurements is likely to be linear.

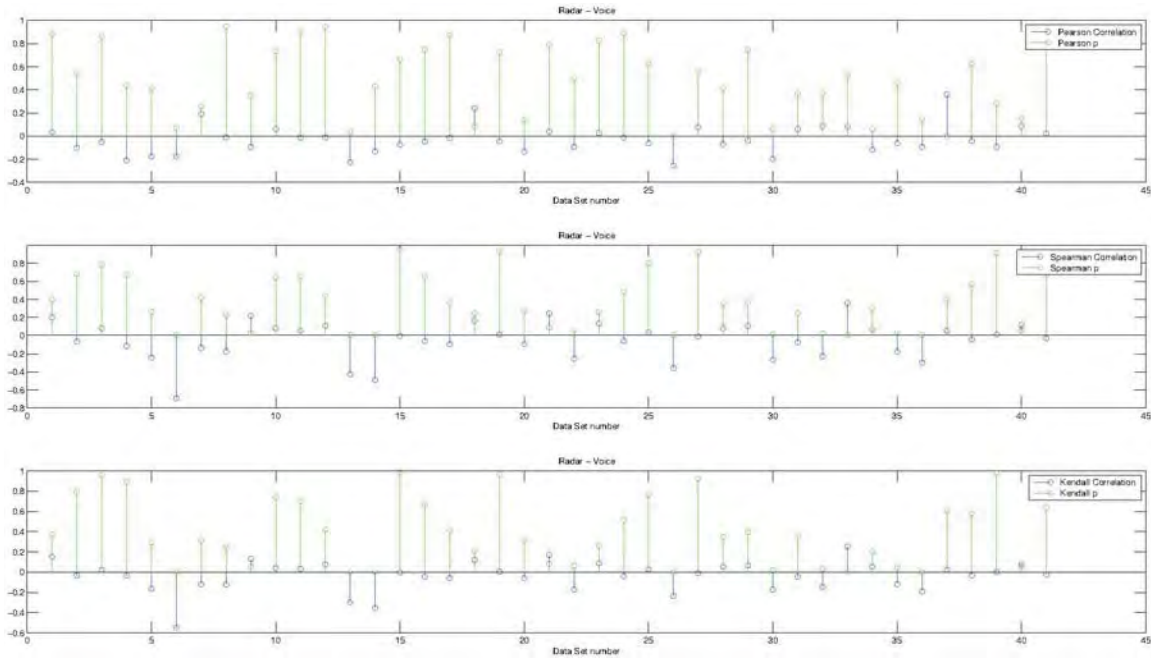


Figure 20. Correlation of Radar and Voice measurements taken at zero lag.

Unlike the Data - Voice correlation, there are some times when the greatest peak is in the anti-correlation. This would indicate that Radar response increases when phone measurements decrease. Also, the strength of the correlation varies more than it did for the Voice - Data correlations. While anticorrelation was not observed in the Voice - Data correlations, the occurrence of it cannot be ruled out. However, it seems more reasonable that with the similarity in the measurement process between the Data and Voice channels, that anti-correlation is unlikely.

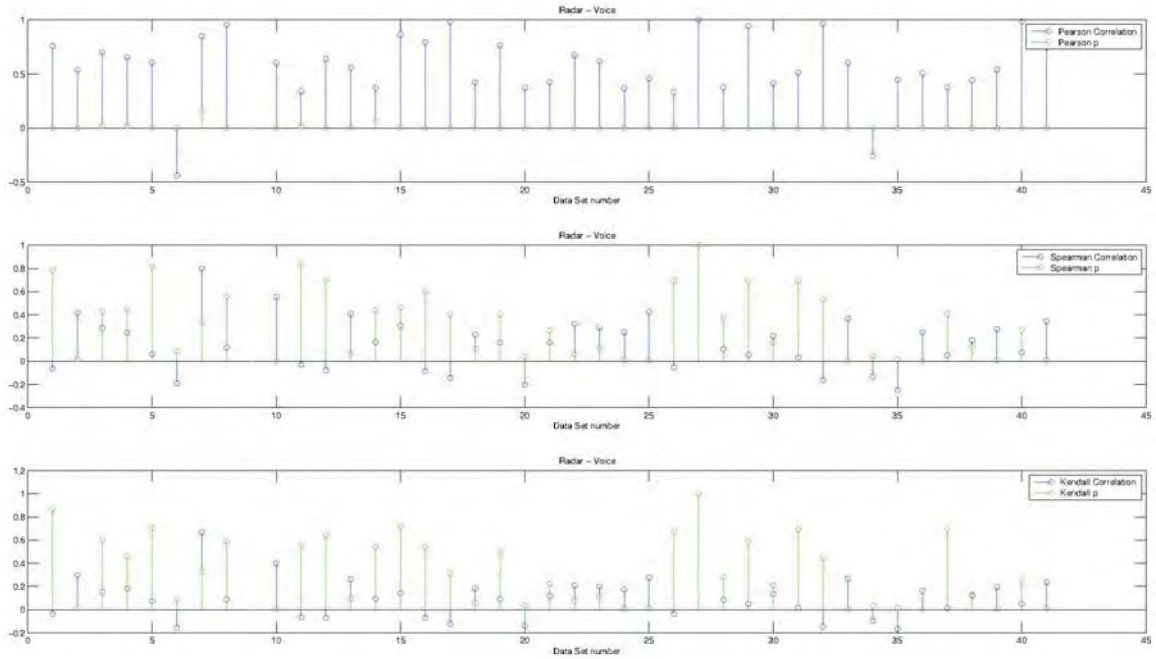


Figure 21. Correlation of Radar and Voice measurements taken at the lag where the cross-correlation peaks.

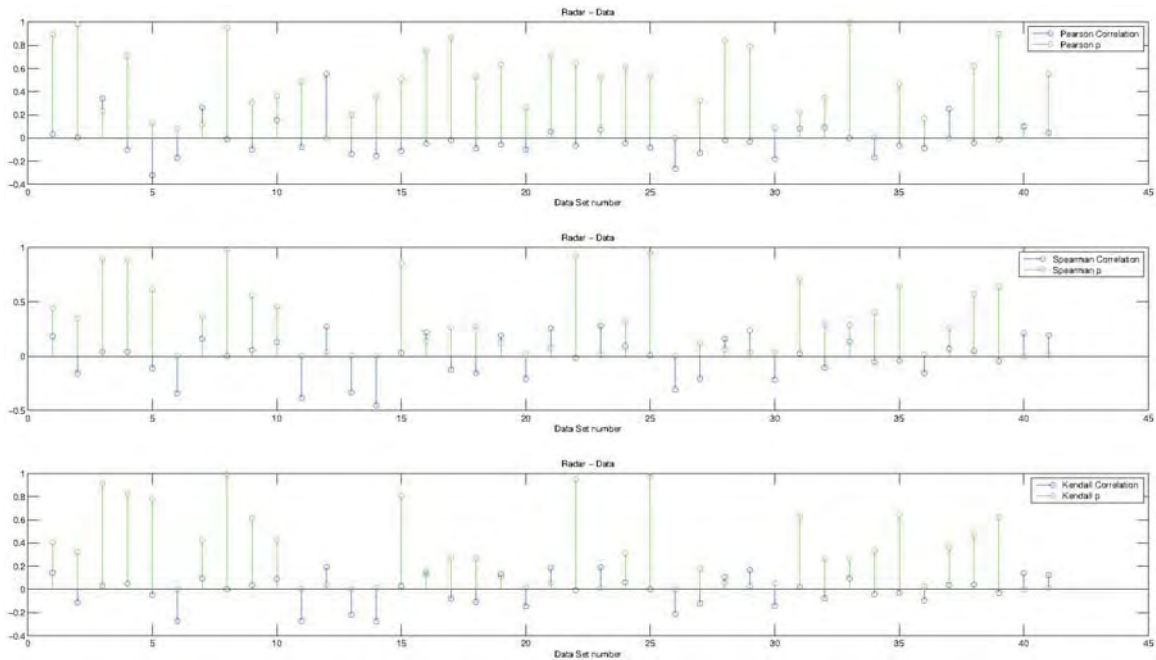


Figure 22. Correlation of Radar and Data measurements taken at zero lag.

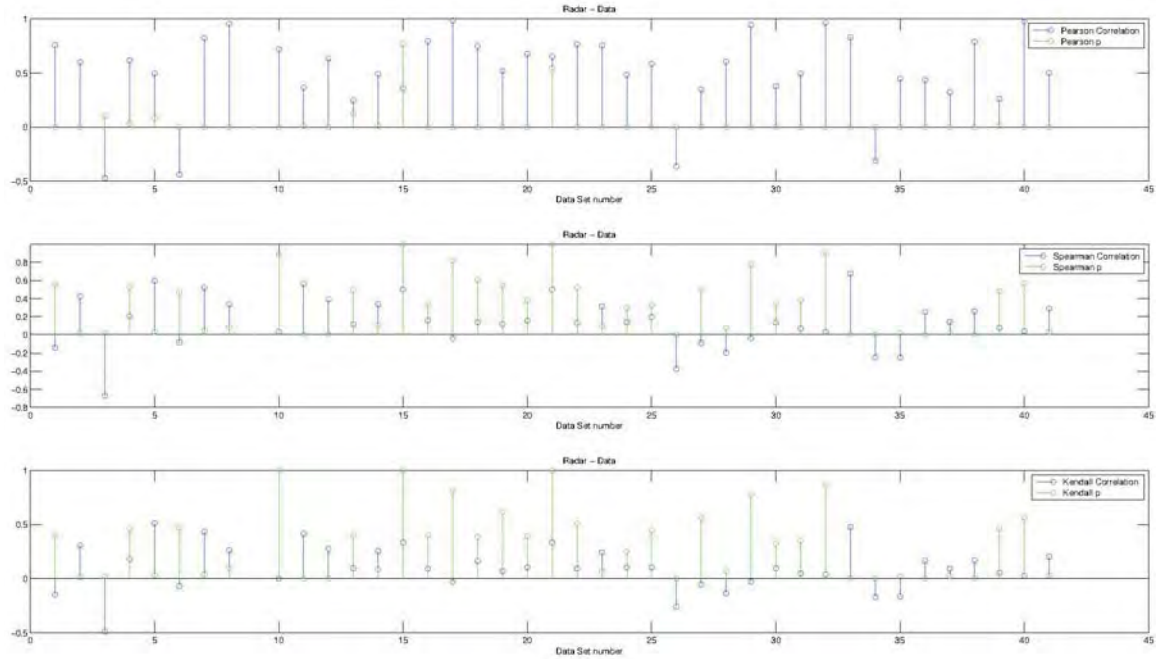


Figure 23. Correlation of Radar and Data measurements taken at the lag where the cross-correlation peaks.

Anti-correlation is uncommon in the Radar - Voice and Radar - Data measurements. In both cases it occurs less than 10 % of the time. The Radar - Data measurements anti-correlate 4 times while the Radar - Voice measurements anti-correlate 2 times. It is not known if the factor of two difference is significant. It may be that multiple processes are competing in the phone measurements, some of which are correlated to Radar measurements and others are anti-correlated. Each type of signal may be different in how strongly it is affected by the correlated and uncorrelated processes. The number of samples is small at 42. With rates of 4 out of 42 and 2 out of 42, both values are less than 1 standard deviation from the average rate, $3/42$. More measurements are needed to provide more confidence in the rate of anti-correlation. Radar - Voice correlations appear to be stronger than Radar - Data correlations, and the Radar-Data shows more anti-correlation.

The ranked correlations show moderate to poor correlation between the Radar - Voice sets and the Radar - Data sets. This, combined with the wider variance in the lag of the cross-correlation peak implies that there are processes that the cross-correlation detects, but ranked correlation does not. Ranked correlation can often detect non-linear relationships, but may not be as sensitive to periodic relationships. For this reason, there may be some periodic effects that the Radar and phone measurements are picking up, but scaling differently. The ranked tests seem to show more anti-correlation as well., but many of these are not statistically significant. Many of the tests show a poor statistical significance for the ranked correlation functions.

Weather Effects

Surface weather observations from a nearby airport were collected for comparison with C_n^2 data. These observations are used to look for patterns in well correlated, and poorly correlated data. A total of six examples will be presented. The examples were selected by looking for points in the cross-correlation plot where the Radar - Voice and Radar - Data sets had strong or weak correlation. Figure 24 shows the correlations from all 42 sets, with the selected points circled. The good correlation points will be discussed first. In all plots, the Radar measurements are in blue, and the Voice and Data measurements are in red. The heavy dashed lines are bezier curves of the data and the lighter lines are the true measurements.

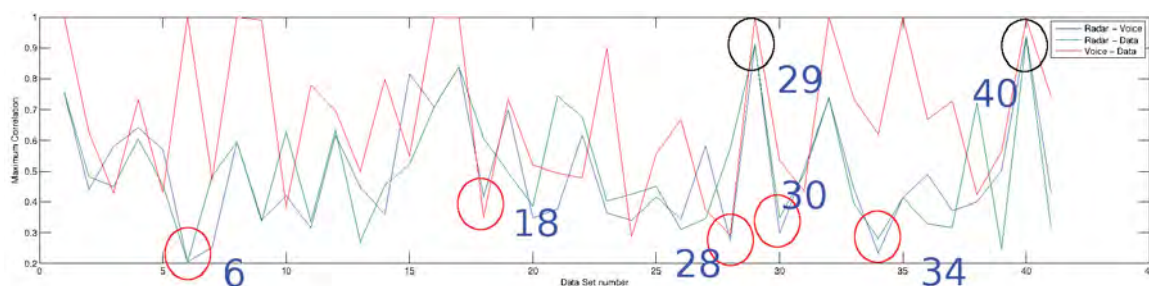


Figure 24. Cross correlation results with the 4 poor correlation plots circled in red, and the two high correlation plots circled in black. The data set numbers are in blue.

Weather During Good Correlation

Two plots of C_n^2 measurements that showed very good correlation are presented in figures 25 and 26. Figure 25 is of the 29th data set. These measurements were taken from 9:30 am until 3:00 pm on August 7. The local weather changed little over this period. The sky was cloudy with light to moderate (7-10 knots) winds. Weather was similar for Figure 26. This is from the 40th data set, beginning after 10:00 pm

on August 27. In both figures, similar features are easily noted between the plots. In Figure 26 the increase in the radar plot at the end of the data file is due to a thunderstorm beginning. The rest of the day was cloudy or partially cloudy. It is not known why both phone plots show a sharp rise at the end of the plots in both figures. A sharp rise or fall is present at the ends of many of the phone plots, but it is not seen in a majority of the plots. There is possibly a bug in the way that C_n^2 is calculated at the beginning and end of the files that makes the initial and final points more sensitive to variation than the rest of the points. This could be artificially increasing or decreasing agreement in some of the plots, but there does not appear to be a connection between correlation strength and the presence of these events. The spikes are seen in highly correlated and poorly correlated data, so it is assumed to create random noise in the correlation measurements that affects the standard deviation of the correlation values, but has little effect on the mean correlation strength.

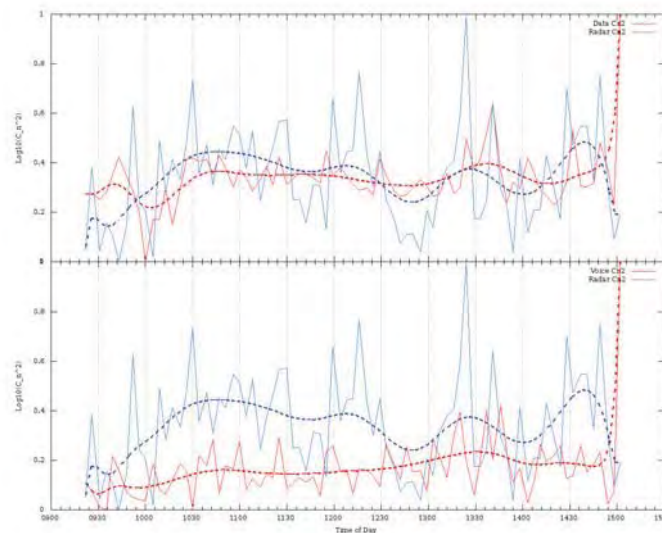


Figure 25. Normalized Radar and phone measurements of C_n^2 taken on August 7th during a time of cloudy skies with light to moderate winds. These plots showed good overall correlation.

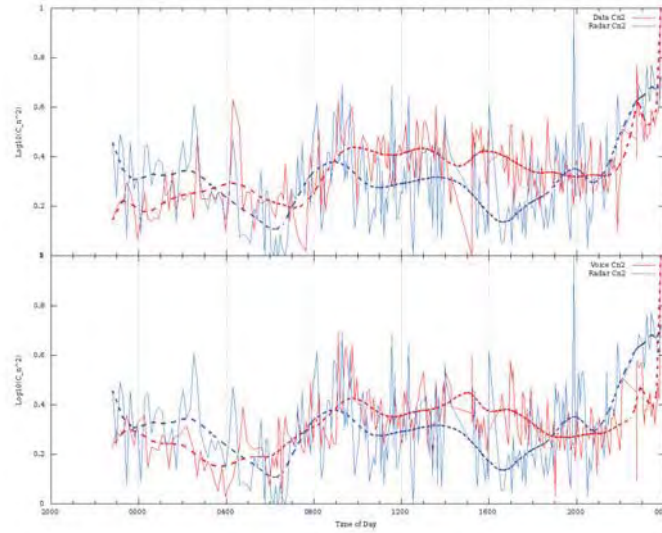


Figure 26. Normalized Radar and phone measurements of C_n^2 taken on August 27th. The plots show good correlation.

Weather During Bad Correlation

While there was a thunderstorm at the end of Figure 25, it happened that the phone plots were also increasing, which likely helped the correlation. In other plots that had rain events, C_n^2 measured from the phone appeared to be unaffected. Because the Radar C_n^3 calculation is based on the reflectivity measured by the radar, rain events appear as strong turbulence in radar plots. These artificial peaks cause the correlation to drop to very low levels. Two examples of precipitation are seen in figures 27, 28. In the first a thunderstorm and rain caused a definite hump. In the second plot, a mist was present for hours, but the radar measurement actually dropped down during this period. Unfortunately, only a few data sets during strong precipitation are available, and number 18 is the only one that has good measurements before and after the storm. It is hard to draw conclusions about how well the phone measures turbulence in the rain, but it is apparent that it does not react the same way as the Radar.

Figure 27 is from August 7. The first part of the day is cloudy with winds at around 9-10 knots. This is followed by a thunderstorm which is evident in the radar returns. Surface observations record a thunderstorm in the vicinity at 4:46 pm, followed by a thunderstorm with rain at 4:50. The shaded region depicts the recorded thunderstorm period. Based on the reflectivity plot, the radar picked up strong returns before the airport recorded the beginning of the rain. This may have been caused by the radar measuring reflections from rain at a higher altitude earlier on, or possibly the rain began at the path before it was reported at the airport.

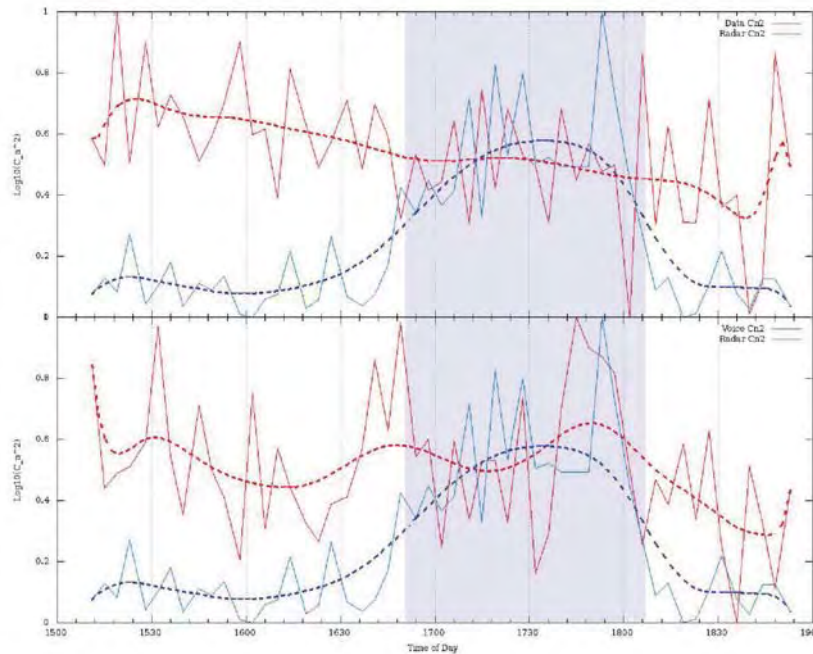


Figure 27. Normalized Radar and phone measurements of C_n^2 . The shaded area indicates a period of reported thunderstorms.

The 28th data set, taken August 7 - 8, is pictured in Figure 28. This plot is interesting because none of the plots correlate well. This plot is from the night after the storm in Figure 27. Sunrise would have been at about 6:42 am. Note

the dip in the radar plot right after this time. Changes in turbulence can usually be seen in both radar and phone data around sunrise, and sunset. In many plots, a change is also seen about an hour or so after sunset. Mist was seen during the shaded portion of the plot. Wind speeds were light, or not detectable all night. A definite relationship between wind behavior and correlation has not been defined, but some trends have been observed. In general, the high correlation plots came from days with frequent variation in wind speed and direction; higher wind speeds; and during 'gusty' periods. Lower correlation plots had lower overall speeds and steady or gradually changing wind speeds. However, there are a few high correlation plots with zero or low winds, as well as low correlation plots with high and variable winds. Wind direction comparisons have not been done.

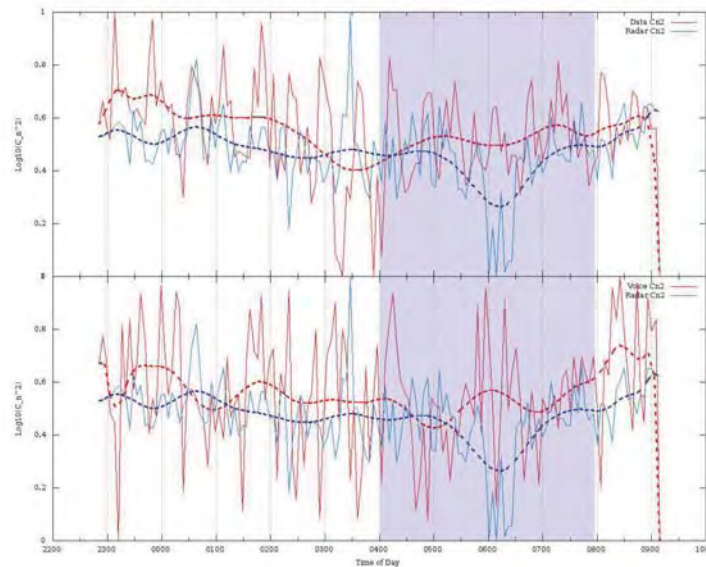


Figure 28. Normalized Radar and phone measurements of C_n^2 . The shaded area indicates a period of reported mist.

Some plots with poor correlation occur during periods of strong winds. Figure 29

is an interesting example because there is a strong peak that appears at about a 25 minute delay between the two sources. The shaded area in this plot corresponds to a period of strong winds. Sustained winds were observed at about 9 knots with gusts up to 17 knots. There are obviously some common features in the Data and Voice channels. The tall, narrow peak appears to happen earlier in the radar plot. There is a low plateau that precedes this peak, but it looks like the plateaus happen earlier in the phone plots. This could be evidence of the radar and phone seeing different aspects of the turbulence, which react at different speeds to outside driving forces like wind gusts. The low wind portion of the radar returns appear to have zero return from the radar. This section likely contributed to the low correlation, and may be caused by turbulence returns being too low to detect with the radar.

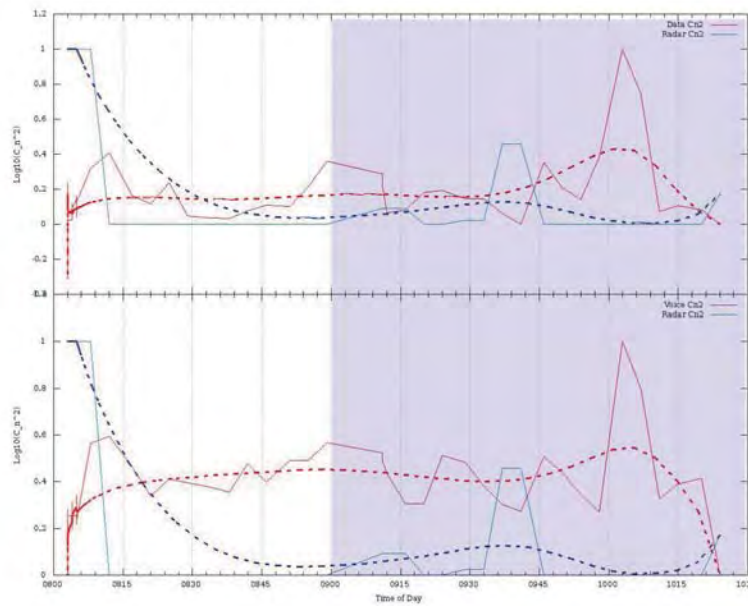


Figure 29. Normalized Radar and phone measurements of C_n^2 . The shaded area indicates a period of strong winds.

Figure 30 is an example of several effects that can degrade correlation. The plot

is from August 26-27. The narrow band is a period of mist, which looks to have come on in morning, after sunrise. Sunrise this day was at about 7:00 am. The radar C_n^2 appears to have dipped during this mist event, like it did in Figure 28. All plots show a drop in turbulence during the night, but the phone drops off just after 2:00 am, while the Radar drops off after 4:00 am. This may be more evidence of the data channels reacting to weather changes at different rates. The sky was clear through this night, with light winds. At the end of the plot, there is evidence of data loss. While there may be a weather condition that causes the phone power to stay constant, this data loss will be assumed to be a bug in the recording device for this work. So the change in reaction time, precipitation, and data loss are all present in this plot.

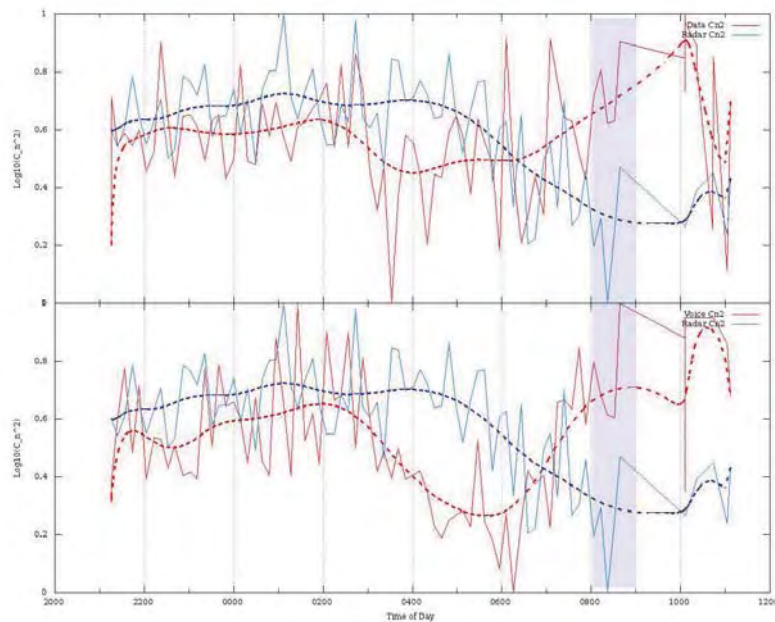


Figure 30. Normalized Radar and phone measurements of C_n^2 . The shaded area indicates a period of reported mist.

Comparison of the plots and local weather events has created some interesting

observations. Large precipitation creates expected spikes in Radar data, but mist appears to cause a dip in returns. Neither seems to have a significant effect on phone scintillation, but agreement in the Voice to Data lines is poor during precipitation. This was expected for the Radar - Voice and Radar - Data plots, but not for the Voice - Data plots.

Plots of the raw phone power are not pictured, but appear to react to weather events like precipitation. So, the overall power can react to weather events, but the scintillation about the mean appears to still be related to turbulence. The ten lowest correlation plots between Voice and Data were compared with the 10 highest correlation plots. General observations of weather conditions during these periods suggests that there may be a relationship between how windy and cloudy it is, and how well the plots agree. Overcast, hazy or misty days appeared to produce good agreement, and strong, variable winds produce good agreement. Clear weather with low winds appears to produce poor agreement.

A similar comparison of the weather during plots of high and poor correlation was done for the Radar - Voice and Radar - Data sets. Definite trends were not as obvious in these plots. An obvious dependence of the correlation on wind strength was not seen. Nor could a relationship between cloud cover and correlation be seen. Precipitation was still associated with poor correlation. None of the correlations showed evidence that they were dependent on file size.

Poor Correlation That May Not Be Directly Related to Weather

Figure 31 is from August 21. The weather was clear, with light but steady winds during the night that dropped off at sunrise to below detectable levels. The very beginning of the plot is from the period just after sunset, which occurred at about 8:25 pm. It can be seen that the phone measurements correlate reasonably well with

each other, but the Radar plots to dot often agree. There is also a period of data loss after 8:00 am. This appears to be caused by large gaps in the phone data. Some measurements in this part of the file have as much as 15 minutes between them. Typical measurements are taken at least every second. All three data sets seemed to show different behavior over the night. The correlation between the Data and Voice channels was still over 0.6, indicating that the phone channels were seeing similar signals. The data loss was likely to reduce the correlation significantly, and it may have be due to non-weather related effects. The loss of data may have been due to turbulence signals becoming too small, which makes them indirectly related to the weather. Since the correlations were high enough to suggest that the cell phone is measuring turbulence, investigations into why some plots did not correlate will be left for future work.

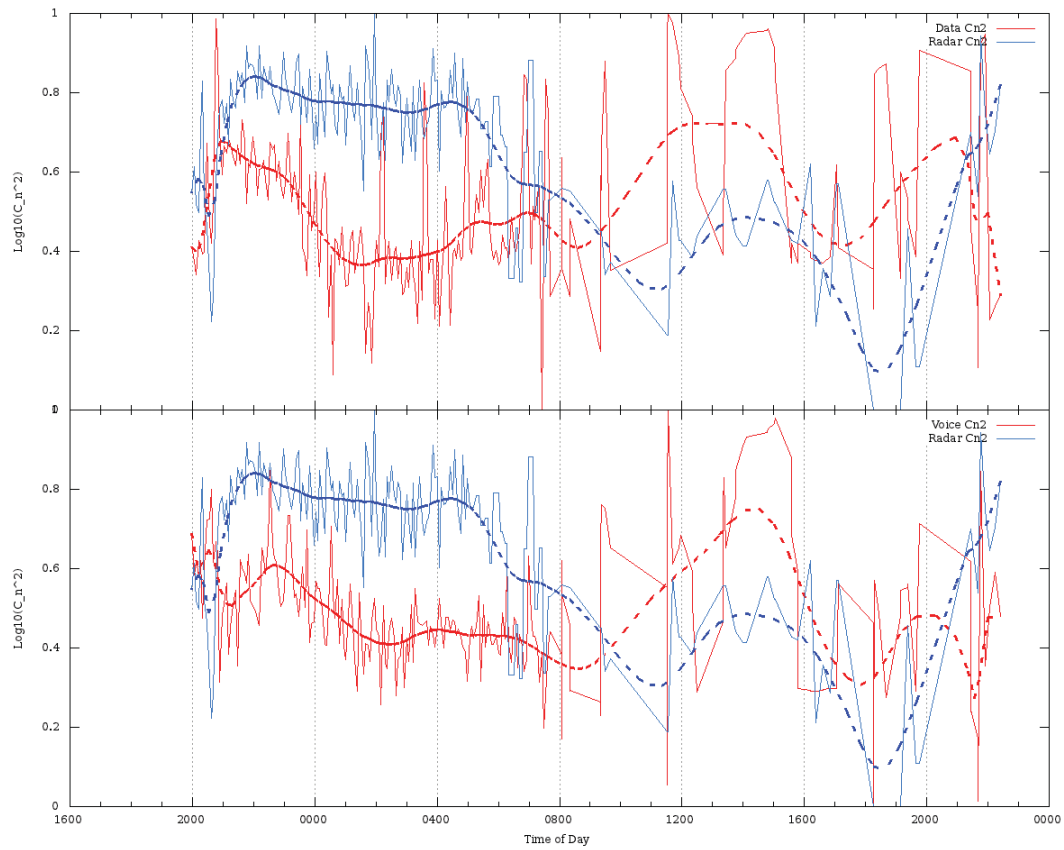


Figure 31. Normalized Radar and phone measurements of C_n^2 . The plot characteristics change dramatically at approximately 7:00 am. This is approximately sunrise, and the wind speed dropped from a steady wind overnight to almost no winds during the day.

V. Conclusions and Suggestions for Further Work

Conclusions

The linear correlations of all 42 files were reasonably strong to very strong, this coupled with the low p-test values indicates that it is very unlikely that the cell phone C_n^2 measurements are not correlated to weather radar measurements. The hypothesis that turbulence along the propagation path is being measured by the phone seems to be a very likely explanation for this correlation. This work certainly suggests that further investigation into this remote measurement method is likely to yield good results, and could eventually lead to a properly calibrated system.

Weather relationships to the various measurement techniques were largely inconclusive. Agreement between both signals from the phone seemed to be best when the weather was cloudy and windy. The Radar and phone measurements did not correlate well during rain. This was expected, but does not do anything to suggest how the phone signal responds in precipitation. Measurement of turbulence in rain may be difficult because the rain would be expected to interfere with microwave and IR scintillometers or temperature based wind probes. However, given the longer wavelength of cell phone signals, it is reasonable to assume that precipitation causes less masking of the turbulence than the shorter wavelength Radar.

The advantage of using the cell phone signals has been that it is relatively easy to collect data over long periods of time. The large amount of data, and the long span over which it was taken has allowed for a strong statistical determination to be made. Furthermore, the lack of expensive equipment makes this investigation easily justified as a preliminary step.

There were also disadvantages to using the cell phone. At times measurements could not be taken because the phone was needed for personal use. Furthermore the

application required large amounts of power, and the phone would quickly discharge if it was not plugged in when taking measurements. From a measurement standpoint, there are several unknowns that prevent proper calibration. The phone's attenuation is not known, nor is the calibration, the signal power measurement method, the data keys being used, the actual bandwidth, the settings of the rake filter, nor the communication frequency. The data logging software was buggy at best, and getting the phone to take long measurements involved careful use of the phone, and a fair bit of luck.

Some of these disadvantages could be overcome with improved programming of the phones. It is likely that the phone can be made to take measurements in a more reliable way. The power requirements could be reduced by allowing the user to turn off the GPS system for periods when the phone will not be moved. Many of these disadvantages can be overcome with dedicated hardware. Having phones that are only used for experimentation and could allow for more continuous measurements over long periods. It may be possible to tap into the phone's hardware and software in order to track the attenuator, band filter, and decode settings. Even more usefulness could be gained from purpose built transmitter and receiver hardware.

Most of the work, in terms of time and effort, were involved in writing the code that can get C_n^2 from weather radar files, and the code that determines how to correlate measurements taken by the phone with the available radar files. The code for extracting the path-averaged reflectivity was written as a set of C header files, using ANSI C and NASA's RSL library. This should allow the code to be integrated into other works.

This work makes significant progress towards providing a real-time passive solution for sensing turbulence on the battlefield. Turbulence measurements of this sort can be done using many types of RF signals in addition to cell signals. Other possible sources

include communications or Radar signals. It may be found that a cooperative signal, like a com link, could be used as a scintillometer in addition to its normal duties with no significant impact on the device functionality. Furthermore, uncooperative signals, like a radar or communications link, may provide a scintillation measurement capability for the line of sight path from a target.

This RF measurement technique could be used to better estimate range and adaptive optics capabilities for directed energy weapons in real time. The wide area coverage of RF signals may allow for a 2D or 3D mapping of the turbulence in a region. These maps may help to predict the turbulence that will be encountered in during an engagement. Finally, this measurement method is inexpensive and provides a mobile, and reasonably persistent measurement capability that traditional scintillometry does not. This could be as asset for adaptive optics testing, providing an instrument for measuring turbulence in an area that is easier to set up than line of sight scintillometers.

Another possible application is improvement of data rates for CDMA digital communications technology. It is quite possible that some encoding schemes will be more susceptible to turbulence than others. If this is true, then frequency allocation rules can be augmented with a turbulence table. This may allow for better apparent signal strength by allowing users that are already contending with weaker signals use the more robust encoding keys. For periods of low turbulence, encoding with a scheme that provides a higher data rate, but requires better SNR may be preferable. The encoding could also be adjusted for periods of strong turbulence: making the signal more robust at a cost of lowering the overall data rate.

Suggestions for Future Work

A logical next step for further work is to improve the calibration of the phone measurements. Several steps will be required to improve our understanding of how turbulence effects cell phone signals. From a hardware perspective, a purpose built measurement instrument is important. This is needed to help remove uncertainties in the signal characteristics, and better investigate the cause of hypersensitivity in the phone.

Verifying CDMA Hyper-Sensitivity

One issue affecting the phone measurement method is uncertainty in why the signal strength varies as much as it does. An experiment to test this can be done with a directive receiver. According to the relationship used for optical scintillometers, the amplitude scintillation should be much less than the measured signal scintillation. A directive receiver pointed at the transmitter should be able to measure the power received on a straight line path from the transmitter. The CDMA signal is noise-like so a measurement of the power received within the band should have much lower scintillation than the cell phone power. This measurement should give a sense of how much of the power variation is from amplitude scintillation, and how much is power from multipath, and phase scintillation. The direction for further research will depend on the results of such a study, so this would be an important next step.

A directive receiver on the phone may also be useful for reducing multipath fading. This may help to increase correlation.

A method for determining the data key would be useful. This could allow for the sensitivity of different keys to be checked. Because of the limited number of keys, a look-up table may be used to determine calibration adjustments based on the key being used. Each tower emits a standard identification and synchronization key. Since

this signal is predictable, and consistent, it may be used to do CDMA measurements without needing an active phone line. This would be a useful key to calibrate because it would be easier to exploit for passive measurement.

A more thorough investigation into the expected effects of propagation on CDMA power would be useful for determining what turbulence parameters are most visible to the phone.

Over time, modifications to Kolmogorov's spectrum have been made that improve the agreement of the theory with observations. The changes focus primarily on behavior of the model at the dissipation range. [2] For this work, the wavelengths involved are 10 cm for radar and about 16 cm for the cell phone. This means that the smallest eddies are smaller than the wavelength being used, so the implications of the newer models may not significantly affect the direct path scintillation calculation. The defocusing process for the cell phone will be based on eddies that are, in general, larger than l_0 . However, the smaller eddies may create scattering in cell phone bands that is not expected for the shorter wavelengths of microwave, IR spectrometers. These scattering effects are noted, but development of scintillation based on them is outside the scope of this work. It is expected that the size of the inner scale eddies and their energy distribution may have a strong effect on calibration of Cell phone measurements. However, the longer wavelengths of the Radar and Cell signals makes them better suited to detection of turbulence that is outside the outer scale of the Kolmogorov spectrum. This may allow for detection and measurement of turbulence over long paths, where saturation makes other scintillation techniques impractical.

Appendix A. CDMA Encoding → Decoding

Due to limitations on the available resources needed for communication, a method must be employed for cell phone companies to be able to divide the available communication capacity among their subscribers. The amount of data that can be sent in a communication channel is dependent on the *Power*, *Bandwidth*, and *Time* available to the channel. There are several strategies that can be implemented to allocate portions of these resources to each user. The resource allocation methods are based on sharing the resource in such a way to reduce interference among the users. The division types can be classified by the resource being shared.

1. Band Division: Dividing the available bandwidth into subsections, and allotting a band to each user.
2. Time Division: Divide the resource use in time and have the users to take turns using the channel.
3. Power Division: Separate the users channels in such a way that the power of each user's channel appears to be acceptably small to other users.

CDMA is a form of the third type of subdivision. In CDMA, users do not subdivide the available bandwidth, nor do they take turns using the bandwidth. Instead, they use a special encoding that allows them to subdivide the available power. Before discussing how CDMA accomplishes the power division, it will be helpful to relate another form of power division, spatial separation. In spatial separation, each channel is separated by a great enough distance that the channels do not interfere. This is easily accomplished by physically separating the Transmitter (Tx) and Receiver (Rx) pairs of each channel from the Tx - Rx pairs of other channels. This can be done either with distance, or with a physical barrier that blocks wave transmission.

CDMA achieves power division using a specialized encoding scheme. Code division reduces the amount of interference that each user receives from other users resulting

in a similar effect to physical separation. The energy of other users adds to the background noise. An example of how this is accomplished is presented below. The underlying theory is based on orthogonality. Each user is assigned a binary code that is orthogonal to all the other users. This code is used as a carrier for the data that is being sent. Since all of the carriers are orthogonal, it is possible to differentiate the users' signal from all the others. So the base station is able to send all of the users' data simultaneously and across the same band. The codes are then used to extract each user's data, with their portion of the total energy, from the ensemble signal that was sent.

For transmission from the base station, synchronous CDMA is used. Production of synchronous CDMA signals involves using a finite set of orthogonal codes. Each user's data is carried by one of these codes. Viterbi gives three requirements for the codes in Chapter 2 of his book. [17]. These requirements call for the CDMA waveform that is transmitted to appear like white noise. For synchronous CDMA the tower broadcasts all of the users' data simultaneously. While each user's data may be a two-level digital signal, the sum of these signals will not look like a digital signal, but will approximate white noise. To see this, consider the sum of the signals from N users at one moment in time, t . Each user's signal at time t is drawn from the set $[-1, 1]$ with equal probability, $P(x = 1) = P(x = -1) = \frac{1}{2}$. The sum y of N draws of x at time t is thus drawn from the set of integers $[-N \leq y \leq N]$ with

$$y = \sum_i^N x_i. \quad (13)$$

This creates a zero mean binomial distribution. So at each time t , the level of the aggregate signal is pulled from a binomial distribution of N trials. It can be shown [17] that this signal, $y(t)$ will look approximately like white noise for large N .

For the power division to work, each code must be orthogonal to all the other

codes. For example, a 4-bit set of codes could be the set in table 2.

Table 2. Some Basic Orthogonal Codes

User No	Code			
1	1	1	1	1
2	1	1	-1	-1
3	1	-1	1	-1
4	1	-1	-1	1

These codes have been converted from the customary binary values of "0" and "1" to "-1" and "1". This step is done because the final signal will be sent out as a set of voltages on an antenna, and should have an average (DC) value of 0. Each user's code can be used to carry data by multiplying the entire code by the value to be carried. For example, the user code [-1 -1 1 1] can be used to carry a binary 1 by multiplying by the vector by 1,

$$[-1 \ -1 \ 1 \ 1] = 1 * [-1 \ -1 \ 1 \ 1]. \quad (14)$$

The same code can be used to carry a -1 by multiplication too.

$$[1 \ 1 \ -1 \ -1] = -1 * [-1 \ -1 \ 1 \ 1]. \quad (15)$$

Each bit of data that is to be sent to a user is combined in this manner with their code. This decreases the data rate by 1/N, where N is the number of bits in the code. However, each user is allowed to use the entire available bandwidth, so their data rate after this reduction is still high. While the user codes go from -1 to 1 in this example, the actual range is varied based on the channel requirements. So the user's code in the example above may be scaled by some value a to be [-a -a a a] where a is

a real number and $a > 0$. The tower will decide how to scale each user's data based on the needs of each channel, and the total power constraints of the tower. Practical CDMA codes are much longer than 4 bits so that many users can be accommodated.

Decoding of the data is done by taking the zero-lag correlation between the received signal and the code. Positive correlation values indicate that a 1 was sent, negative correlation values indicate a -1, and zero correlation indicates that no data was sent. An illustrative example of encoding and decoding data is presented below. This example is simplified from practical techniques so that the encoding and decoding method can be presented. For this example the digital word for the ascii letter 'a' will be sent. It is composed of 8 bits: 0110 0001. This letter will be combined with three users' signals. The total data package will require $8 \times 4 = 32$ bits total.

First, the data is expanded to match the length of eight codes.

Table 3. The binary word 0110 0001 expanded out for encoding.

0000	1111	1111	0000	0000	0000	0000	1111
------	------	------	------	------	------	------	------

Next, it is combined with a user's code in XOR logic, and converted to "-1", "1" binary.

Table 4. An example of encoding the binary word 0110 0001 with the user code 1001.

Data	0000	1111	1111	0000	0000	0000	0000	1111
Code	1001	1001	1001	1001	1001	1001	1001	1001
XOR	1001	0110	0110	1001	1001	1001	1001	0110
Conversion	1-1-1 1	-1 1 1-1	-1 1 1-1	1-1-1 1	1-1-1 1	1-1-1 1	1-1-1 1	-1 1 1-1

Then, the codes from all the users are summed up.

Table 5. Combining several users' signals into one signal.

User 1	1-1-1 1	-1 1 1-1	-1 1 1-1	1-1-1 1	1-1-1 1	1-1-1 1	1-1-1 1	-1 1 1-1
User 2	-1-1 1 1	-1-1 1 1	1 1-1-1	-1-1 1 1	-1-1 1 1	-1-1 1 1	-1-1 1 1	-1-1 1 1
User 3	-1 1-1 1	-1 1-1 1	1-1 1-1	-1 1-1 1	-1 1-1 1	-1 1-1 1	1-1 1-1	1-1 1-1
Signal	-1-1-1 3	-3 1 1 1	1 1 1-3	-1-1-1 3	-1-1-1 3	-1-1-1 3	1-3 1 1	-1-1 3-1

After Reception, the inner product of each user's code is taken with the signal, positive values indicate a binary 0, negative values indicate a binary 1, and zeros would indicate no data.

Table 6. Decoding Data

Word	Code	Dot Product	Binary Value
-1-1-1 3	1-1-1 1	4	0
-3 1 1 1	1-1-1 1	-4	1
1 1 1-3	1-1-1 1	-4	1
-1-1-1 3	1-1-1 1	4	0
-1-1-1 3	1-1-1 1	4	0
-1-1-1 3	1-1-1 1	4	0
1-3 1 1	1-1-1 1	4	0
-1-1 3-1	1-1-1 1	-4	1

The decoding step in CDMA signals may affect power measurements. The process is easiest to describe in frequency space. While the environment is nearly identical for each frequency in the band, there will be some differences. As the power and phase in each frequency component of the signal changes, the correlation strength will tend to decrease. It is proposed that the signal power is based on the correlation strength, so changes in the correlation strength will manifest themselves as changes in

the signal strength. Phase and amplitude changes in each frequency component will reduce the correlation strength of the signals, and appear as power loss because the highest correlation is for identical signals, and all other correlations must be equal to or less than this value. [11]

The RF propagation model is also significantly different from the beam model of LASER and Microwave Scintillometers. The cell phone signal often arrives from several paths after one or more reflections. Each of these paths will have passed through turbulence separated by more than the correlation length. So each path is sampling statistically independent turbulence. For each frequency component in the signal, the apparent lengths of each path will be different. This is compounded by the fact that the base station uses a phase array to steer the beam, and thus the direction of the initial beam will be slightly different for each frequency. The resulting interference at the receiver may be different enough across the band of the signal to significantly affect the correlation strength of the received signal with the user's code.

It is not yet known how significant the interference variation across the band is. It has been seen that the data and voice signals sometimes show independent variation. This suggests that the signals may have different sensitivity to turbulence. Each code has a different frequency representation, and may thus have a different interaction with the environment. Another explanation for the different responses may be that the turbulence effect is not much stronger than other processes, and in weak cases these other (and possibly uncorrelated) processes begin to dominate. Further investigation of these effects will be easier with purpose built hardware.

Appendix B. Phone Logging Application

Programming of the Android® logging system was done using the Android SDK. The Android OS has some major differences from other Linux OS distributions. These differences affected how the data logging application was implemented.

In a typical OS, there is a user account for each person that will be using the device. Several users can be logged onto the same device, but their programs and many of their documents are separate from each other. There are also system accounts, which are similar to user accounts, but are meant for programs that are automatically loaded and controlled. For each user that is logged in, their resources (files, processor scheduling, and the like) is made available to open applications. This can be a security risk because an application can access resources that belong to other applications. In the Android OS, each application is assigned its own user account. This helps to isolate the program from other programs and the OS. In addition to separate accounts, each application is launched into a *virtual machine*. The virtual machine is controlled by an underlying program that can present system resources to each application as needed.

Because of this user structure, access to the phone signal power and location are provided using a *broadcast receiver*. The broadcast receiver is turned on and listens for system-wide announcements sent from the GPS, and phone signal power services. When these services broadcast, then the program can choose to act. This process is depicted in Figure 32

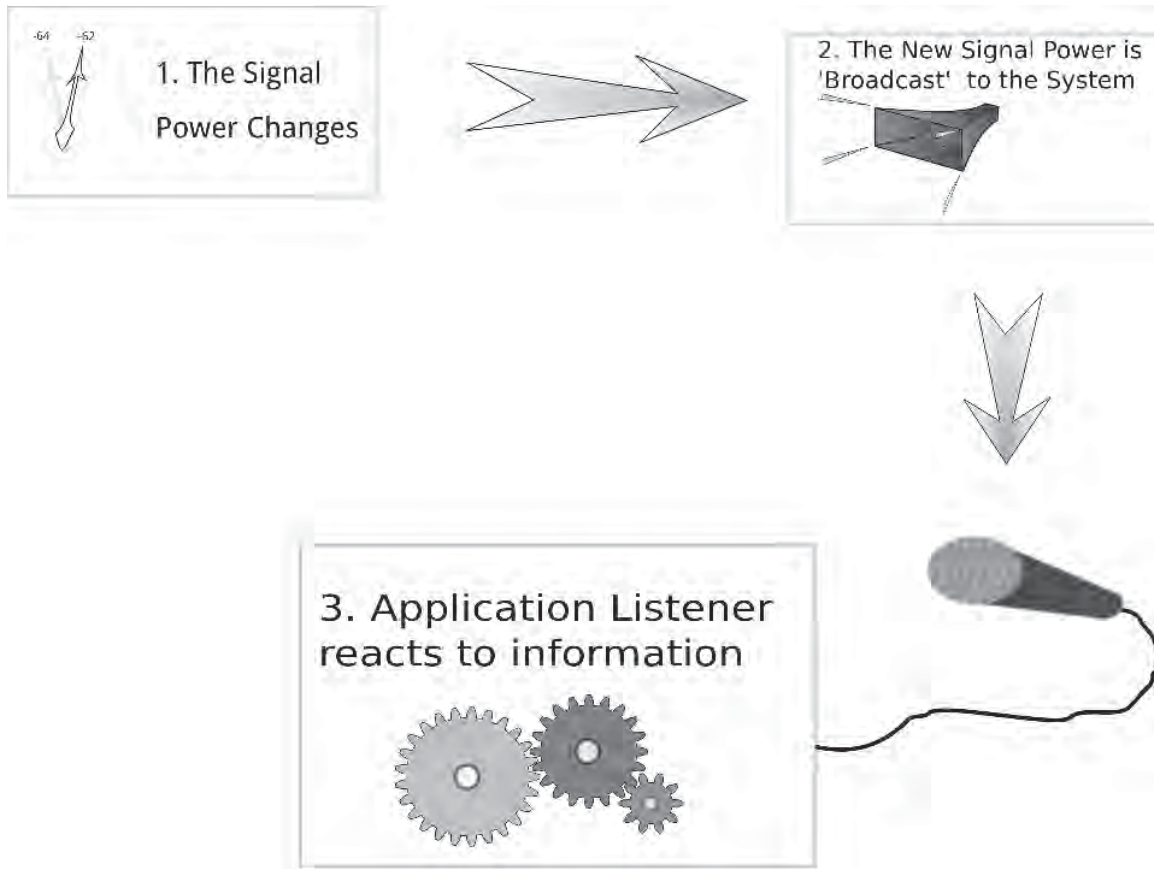


Figure 32. Cartoon of the process by which the Android phone updates the power level to the data logging software.

A consequence of this process is that the logging application cannot request the data on a regular time interval. Each data record is taken in response to a change in the signal level. So the sampling rate varies randomly from sample to sample. This is undesirable for an instrument that is attempting to take discrete samples of a continuous variable. Among other problems, this sampling method leads to undesirable gaps in the data record.

The GPS system in the phone works in a similar manner to the power level monitor. When the data program is started it requires GPS updates. In order to get them, it broadcasts a request for GPS information to the OS. The OS then

turns on the GPS receiver. The GPS receiver is its own program that runs in the backgrounds and updates the phone's position with a system broadcast. The logging application runs a listener. When the listener hears an broadcast from the GPS, it reacts according to the information in the broadcast. In most cases this ends up causing an update in the data lag. Other cases are typically error messages, and are handled accordingly.

Each broadcast from the phones power level monitor includes the power level of the voice and data connection. This is true even if only one or the other has changed. The broadcast also includes information about the *base station* location and ID number. All of this information is recorded along with the system time, the phone location, and the estimated path length. The information is stored in a text file. The file names have a standard format that includes the time the file was created. The text files are stored in the phone's external storage. This allows them to be easily accessed.

It was noticed that there are very large gaps spanning more than an hour in some of the logs. It was also noticed that the application occasionally shut down on its own. Additional debugging time has not been spent to fix these issues. A hard drive crash and poor backup procedures resulted in loss of the source code for the logging software. If time is available, the author intends to re-write the software, but the original source code for the data logging application is not currently available.

Appendix C. Radar Data Extraction Library

The Radar library functions were adopted directly from a method developed by the CDE for measuring C_n^2 from weather Radar returns. The function relating the path averaged reflectivity to C_n^2 is given in Chapter III equation 10. Chapter III also discusses the idea of the path averaged reflectivity. This section will go into more detail of how the new library finds the proper Radar file, and extracts the path averaged reflectivity.

Radar files for the summer were downloaded and indexed. The index file is a text file with the time stamp of every radar image recorded, the path to the tarball containing the compressed images, and the image file name. This was done so that the calling program can find and extract the proper image file, based on when it was recorded.

Radar files are organized based on a hierarchy of objects. Details of the radar structures are available on NASA's TRMM RSL website. [14] On the top level are several different types of measurements called *radar volumes*. For this work, the reflectivity volume was used. Each Volume is then broken up in vertically stacked rings called *radar sweeps*. The sweeps are then broken up in the azimuthal direction into *radar rays*. Each ray is then subdivided by range increments into *bins*. In Figure 33 the lowest elevation sweep is depicted showing the bins and rays of a clear air return. A cartoon of a 3-D sweep is presented in Figure 34

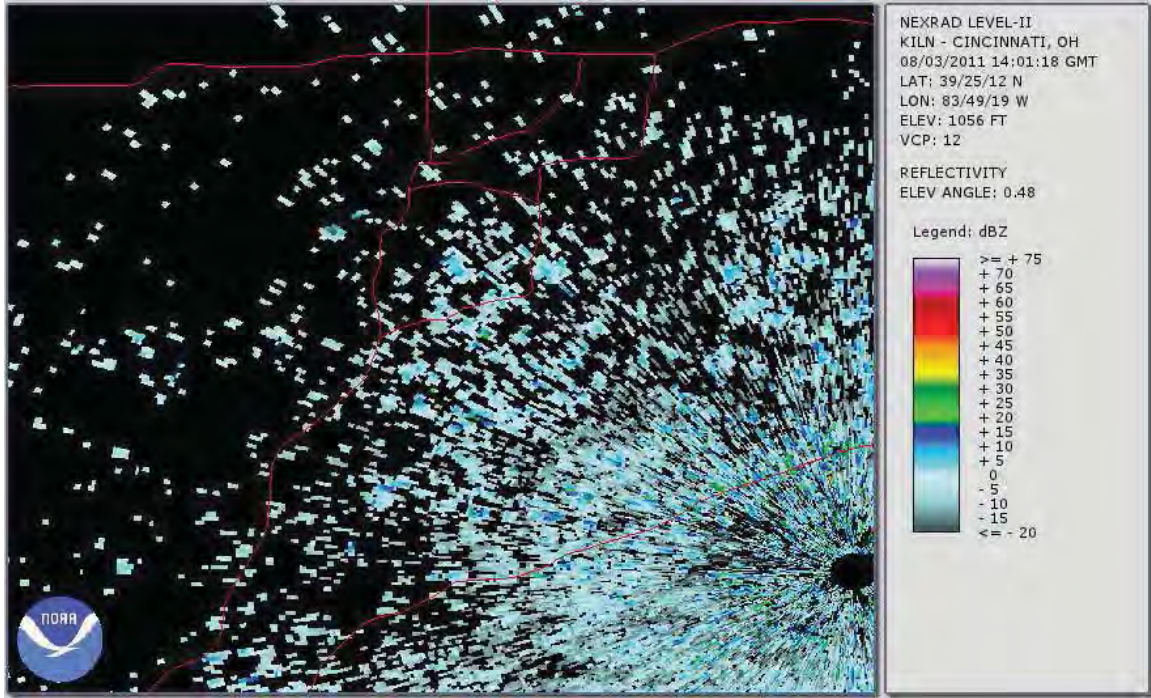


Figure 33. Wilmington NEXRAD Radar image showing clear air returns from the Miami Valley region. The red lines are major highways in the area.

Radar images do not have standard spacings for the sweeps, rays and bins. Each volume that is opened has information about the number of sweeps, and their spacing. Each sweep, when opened has information about the number of rays, and their spacing. The number of rays can be different in every sweep within a single file. Bins are similar to rays and sweeps in that each ray may have different bin spacing, with different initial distances, and different numbers of bins. Furthermore, there are missing bins, rays, sweeps and volumes. In order to prevent crashes, it is important to check each element and make sure that it is not empty before trying to access the data.

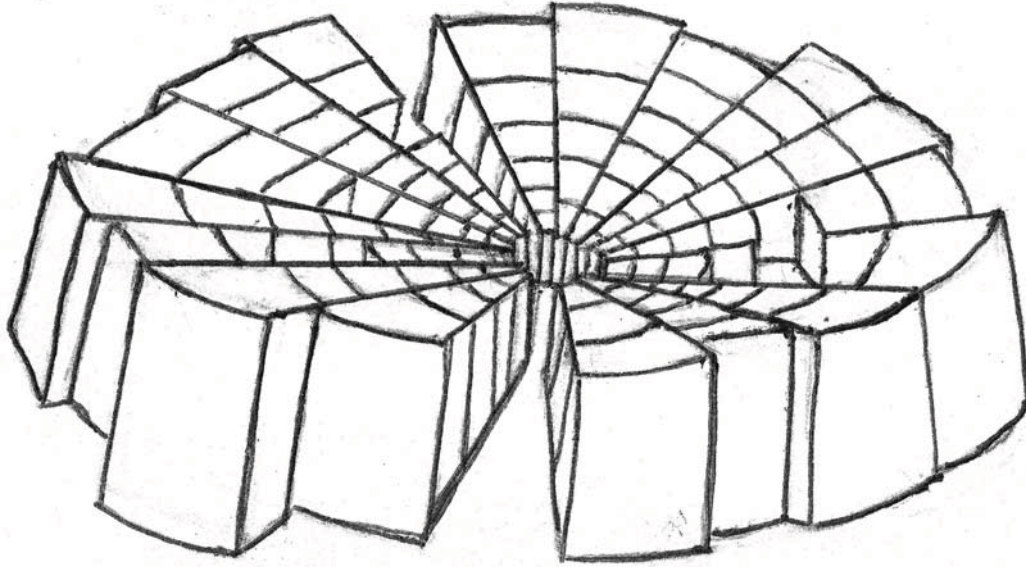


Figure 34. Cartoon of a weather radar sweep. The azimuthal divisions of the sweeps are rays, and the radial divisions of the rays are bins. In each radar sweep it is possible for rays or bins to be missing. Also the spacing and number of bins varies from ray to ray, the spacing and number of rays varies from sweep to sweep.

The lack of a constant or defined structure made the automation code rather complicated. The process for determining the path is outlined below. The author and committee chair will maintain a copy of the C library. A copy may be requested by contacting Dr. Fiorino or Lee Burchett at the CDE in the Engineering Physics department of AFIT.

Once the radar file is opened, and the path has been defined, a starting bin is found. The point is converted into a radial distance with azimuth and elevation. The elevation of the starting point is used to determine the most likely starting sweep, ray, and bin. This bin is found, and the point where the path exits this bin is calculated. That point is used to determine which bin the path goes into next. Once this bin is found, the exit point is calculated, and the next bin is found. This continues until the end of the path is found.

For each bin that the path passes through, the length of the path segment in that bin is calculated. This length, len_i , is then used to determine how strongly the bin's reflectivity, R_i will be weighted when determining the path averaged reflectivity, $R_{average}$. So for a path of length L_{total} passing through N bins, the total path averaged reflectivity is

$$R_{average} = \sum_i \frac{len_i}{L_{total}} R_i. \quad (16)$$

Which was given before as equation 9.

Null bins are not counted toward $R_{average}$, and the length, len_i , that the path passes through while in that bin is subtracted from L_{total} . This is done so that the null bins do not affect the path averaged reflectivity. Most of the complexity is in the checks and estimation of where the path will go next. Adjacent rays and sweeps do not necessarily have the same spacing structure. So, if the path exits into another ray or sweep, then the new ray or sweep must be opened and the entrance point must be searched for. This is compounded by the fact that some rays, bins, and sweeps are empty. The entrance and exit points and path length are all calculated with the true bin structure, which is similar in shape to a spherical $\Delta r, \Delta \theta, \Delta \phi$ sector. In some cases, the entire path passes through empty data, or possibly is in just one bin. The radar libraries attempt to hide all of this behind a simple function that is passed the radar file name, and the path endpoints. This should allow for integration with other systems.

Glossary

absolute temperature is the temperature of the air at its current pressure. This is the measure of the average kinetic energy of all of the molecules in the air.. 9

base station is sometimes referred to as a cell-tower, but is not always a tower. Base stations are the physical transceiver and antenna(s) that communicate with users in a wireless communication 'cell'.. 3, 19, 25, 80

bin is the smallest 3-D element from a radar sweep. Each bin is depicted as having a constant measured value throughout.. 30, 81

boundary layer is sometimes referred to the planetary boundary layer and is the layer of the atmosphere that extends from the ground up to the lowest level of the geostrophic winds. It is the layer in which shear stress between the constant geostrophic winds and the stationary air at the surface in combination with the buoyant motion of air heated by the ground and Coriolis forces cause a constantly turbulent environment.. 1, 8, 13

broadcast receiver is a type of object available to Android applications. The receiver listens for system broadcasts of a certain type. When it hears a broadcast, the listener can trigger execution part of an application's code.. 78

dispersion is the process by which EM waves at different frequencies are made to propagate at different speeds. Dispersion results in the various frequency components of a signal arriving at different times often via different paths.. 16, 21

dispersive is the quality of materials whose index of refraction is not 1 which causes the speed of the wave's propagation to vary with the frequency of the wave. This

leads to problems in sending data because the various frequency components of a signal can arrive at the receiver at different times, leading eventually to a loss of signal for long propagation paths.. 13

potential temperature is the temperature that the air would be if it were brought to standard pressure, 1000 millibars, without adding or removing heat.. 9

radar ray is a line of radar bins extending out in a line from the center of the radar image.. 81

radar sweep is the aggregate of radar rays at one elevation. Several sweeps are stacked vertically to create one radar volume.. 81

radar volume is the 3-D aggregate of data bins of the same measurement type taken from a radar scan. Each radar file contains several volumes for the types of measurements available to the radar. Measurement type examples include reflectivity, velocity, spectrum width, corrected reflectivity, and received power.. 30, 81

relative humidity is the ratio of the pressure that all the water would have if it alone occupied the volume, to the vapor pressure of water at the temperature and pressure of the air.. 9

scintillation is rapid changes in power received over a period of time.. 5

structure constant is a number that describes the average variation in a measurable quantity within a unit volume. . 5

virtual machine is a simulated computer. Virtual machines are run on a 'host' computer and use software to simulate computer hardware that 'guest' software can be installed on. The virtual nature allows for the host to control the amount

of memory and the devices that the guest can see. The guest does not see the host OS, and is only aware of the virtual devices that are presented to it.. 78

water mixing ratio is the ratio of the mass of water to the mass of air.. 9

Bibliography

1. Bennett, C. A. *Principals of Physical Optics*. ISBN 13 978-0-470-12212-9. John Wiley and Sons, 2008.
2. Blaustein, C. G., N. & Christoddoulou. *Radio Propagation and Adaptive Antennas for Wireless Communication Links*. John Wiley & Sons, Inc., Hoboken, New Jersey, 2007.
3. Brown, Robert A. *Fluid Mechanics of the Atmosphere*. Academic Press, San Diego, California, 1991.
4. Commision, United States Federal Communication. "Electronic Code of Federal Regulations". Online Database, December 2011. Part 25.204, section (a).
5. Commission, Federal Communications. "Cellular Transmitter Licensing Database". Online Database, August 2010. [Http://wireless.fcc.gov/geographic/data/db/cellular.zip](http://wireless.fcc.gov/geographic/data/db/cellular.zip).
6. Doviak, D. S., R. J. & Zrnic. *Doppler Radar and Weather Observations*. Academic Press, Inc., San Diego, California, 1993.
7. Fiorino, et al., S.T. "Broad-Spectrum Optical Turbulence Assessments from Climatological Temperature, Pressure, Humidity and Wind". *Journal of Directed Energy*, 3:223–238, 2009.
8. Fiorino, R.M.; Downs A.D.; Bartell R.J.; Krizo M.J.; S.T.; Randall and S.J. Cusumano. "Three-Dimensional Optical Turbulence Assessments from Doppler Weather Radar for Laser Applications". 6th DEPS Systems Symposium, March - April 2011.
9. Ishimaru, A. *Wave Propagation and Scattering in Random Media*. Academic Press, New York, New York, 1978.
10. Jacobson, M. Z. *Fundamentals of Atmospheric Modeling*. Cambridge University Press, New York, second edition, 2005.
11. Kay, Steven. *Intuitive Probability and Random Processes Using Matlab*. ISBN 13 978 0 387 24157 9. Springer, 2006.
12. Langton, Charan. *CDMA Tutorial*. Technical report, www.complextoreal.com, 2002.
13. Meijninger, W.M.L. *Surface fluxes over natural landscape using scintillometry, The scintillation method*. Ph.d. thesis, Wageningen University, Wageningen, the Netherlands, 2003. See also: <http://edepot.wur.nl/121454>.

14. Mission, NASA Tropical Rainfall Measurement. "Radar Software Library". Website, August 2011. http://trmm-fc.gsfc.nasa.gov/trmm_gv/software/rsl/.
15. Tatarskii, V. *The Effects of The Turbulent Atmosphere on Wave Propagation*. translation, Published for NOAA by the Department of Commerce and the National Science Foundation, Washington D.C., 1971. Israel Program for Scientific Translations.
16. Verdeyen, Joseph T. *Laser Electronics*. Prentice-Hall Inc., Englewood Cliffs, New Jersey, second edition, 1981.
17. Viterbi, A. J. *CDMA:Principals of Spread Spectrum Communication (1 ed.)*. Prentice Hall, 1995.

REPORT DOCUMENTATION PAGE				Form Approved OMB No. 074-0188	
<p>The public reporting burden for this collection of information is estimated to average 1 hour per response, including the time for reviewing instructions, searching existing data sources, gathering and maintaining the data needed, and completing and reviewing the collection of information. Send comments regarding this burden estimate or any other aspect of the collection of information, including suggestions for reducing this burden to Department of Defense, Washington Headquarters Services, Directorate for Information Operations and Reports (0704-0188), 1215 Jefferson Davis Highway, Suite 1204, Arlington, VA 22202-4302. Respondents should be aware that notwithstanding any other provision of law, no person shall be subject to a penalty for failing to comply with a collection of information if it does not display a currently valid OMB control number.</p> <p>PLEASE DO NOT RETURN YOUR FORM TO THE ABOVE ADDRESS.</p>					
1. REPORT DATE (DD-MM-YYYY) 22-03-2012		2. REPORT TYPE Master's Thesis		3. DATES COVERED (From - To) June-2010 -- March-2012	
4. TITLE AND SUBTITLE Turbulence Measurement In The Atmospheric Boundary Layer Using Cellular Telephone Signals				5a. CONTRACT NUMBER	
				5b. GRANT NUMBER	
				5c. PROGRAM ELEMENT NUMBER	
6. AUTHOR(S) Lee R. Burchett, Civilian				5d. PROJECT NUMBER	
				5e. TASK NUMBER	
				5f. WORK UNIT NUMBER	
7. PERFORMING ORGANIZATION NAMES(S) AND ADDRESS(S) Air Force Institute of Technology Graduate School of Engineering and Management (AFIT/EN) 2950 Hobson Way WPAFB OH 45433-7765				8. PERFORMING ORGANIZATION REPORT NUMBER AFIT/APPLPHY/ENP/12-M01	
9. SPONSORING/MONITORING AGENCY NAME(S) AND ADDRESS(ES) High Energy Laser Joint Technology Office (Mr. Mark Neice) 901 University Blvd SE Albuquerque, NM 87106 (505)248-8205, Mark.Neice@jto.hpc.mil				10. SPONSOR/MONITOR'S ACRONYM(S) HELJTO	
				11. SPONSOR/MONITOR'S REPORT NUMBER(S)	
12. DISTRIBUTION/AVAILABILITY STATEMENT DISTRIBUTION A: APPROVED FOR PUBLIC RELEASE; DISTRIBUTION UNLIMITED.					
13. SUPPLEMENTARY NOTES					
14. ABSTRACT A new method for measuring the intensity of turbulence in the planetary boundary layer was investigated. Measurements taken using the new method showed high correlation with measurements from weather radar. This method takes measurements of cell phone signal strength and uses scintillation in the signal to estimate the strength of local turbulence. Using cell phone signals provides unique measurement advantages: it is a passive measurement method, it is not strongly affected by precipitation, and one device can potentially measure several paths at once. The measurements were taken using an Android cell phone running a custom built application. The strength of turbulence was quantified using the index of refraction structure constant C^2_n . The goal of the investigation was to determine if C^2_n values calculated from the cell phone signal power show a relationship to C^2_n measurements taken using clear air Radar returns from the communication path. The strength of the agreement between measurements made by the new method and those done with an established method lead to a conclusion that turbulence changes can be measured using cell phone signals.					
15. SUBJECT TERMS Planetary Boundary Layer, Turbulence, Scintillation, Atmospheric Propagation					
16. SECURITY CLASSIFICATION OF:		17. LIMITATION OF ABSTRACT	18. NUMBER OF PAGES	19a. NAME OF RESPONSIBLE PERSON	
REPORT	ABSTRACT			c. THIS PAGE	Dr. Steven Fiorino
U	U	U	109	19b. TELEPHONE NUMBER (Include area code) (937) 255-3636, x4506; Steven.Fiorino@afit.edu	

Standard Form 298 (Rev. 8-98)

Prescribed by ANSI Std. Z39-18